

## Sensitivity of Land–Ocean Circulations, Precipitation, and Soil Moisture to Perturbed Land Surface Albedo\*

BRENT M. LOFGREN

*Great Lakes Environmental Research Laboratory, Ann Arbor, Michigan*

(Manuscript received 17 August 1994, in final form 25 April 1995)

### ABSTRACT

Using general circulation model experiments, it was found that thermally induced overturning circulations that flow between oceans and land at low latitudes can be affected by perturbations to the land surface albedo. When surface albedo is reduced over land at low latitudes, radiative heating of the surface is increased and additional heat is transferred from the surface to the atmosphere, which is largely offset by adiabatic cooling associated with upward motion. This enhanced upward motion is associated with greater low-level convergence of air over the continents, compensated by divergence over the oceans. The enhanced flux of water vapor onto the continents due to this pattern further enhances the thermal forcing through the release of latent heat. In these low-latitude regions with reduced surface albedo, precipitation and soil moisture are increased. Qualitatively opposite effects are obtained by increasing surface albedo.

In midlatitude regions, circulation and precipitation are not significantly affected by land surface albedo. However, decreased surface albedo does increase the amount of heat available at the surface for evaporation. This greater heat availability depletes soil moisture earlier in the season. Again, qualitatively opposite effects are obtained by increasing surface albedo.

Similar perturbations in land surface albedo are used as an analog to the effects of low-level atmospheric aerosols, which have been proposed as a mechanism that may presently be offsetting CO<sub>2</sub>-greenhouse warming. The resulting temperature changes are compared with those occurring in an increased CO<sub>2</sub> simulation.

### 1. Introduction

The fluxes of energy, moisture, and momentum at the atmosphere's lower boundary are major factors in determining its motion, temperature, and precipitation. The characteristics of land and ocean surfaces impact the overlying atmosphere by regulating these fluxes. Thus perturbations in surface characteristics can change climatic variables. The surface albedo, along with other surface characteristics, is strongly influenced by vegetation. Since natural vegetation is dependent on the local climate, there is the possibility of feedback between the vegetation at the surface and the atmosphere overlying it if climate is sensitive to surface albedo. The objective of this study is to test for sensitivity of climate to perturbed surface albedo, and that of a related paper (Lofgren 1995) is to see what role natural vegetation and climate have in sustaining one another.

A number of previous experiments have used general circulation models (GCMs) and other models in which

surface albedo has been perturbed (Charney 1975; Charney et al. 1977; Chervin 1979; Carson and Sangster 1981; Sud and Fennessy 1982; Cunnington and Rowntree 1986; Sud and Molod 1988). These authors have shown that perturbed land surface albedo leads to changes in precipitation by directly altering the flux of solar radiation reflected from the surface, which leads to changes in net radiative heating of the surface and in the fluxes of sensible and latent heat. The mechanism proposed by Charney (1975) and refined in succeeding studies is that higher surface albedo results in relative cooling and descent of the air over the affected region, inhibiting precipitation. Charney also proposed that this would lead to a positive feedback between vegetation and climate in the Sahel.

However, soil moisture, as an indicator of the balance between supply and demand for moisture, is a better indicator of the potential for plants to grow than precipitation alone. In addition to changes in precipitation, changes in potential evaporation resulting from surface albedo perturbations can be important in determining the net effect on soil moisture. For instance, increasing surface albedo may decrease the absorbed solar radiation and decrease the amount of energy available for evaporation from the surface (i.e., the moisture demand). This would partially offset or even reverse the effect of decreased precipitation (moisture supply). Although some of the studies cited above in-

---

\* Great Lakes Environmental Research Laboratory Contribution Number 923.

---

Corresponding author address: Dr. Brent M. Lofgren, NOAA/ERL, 2205 Commonwealth Blvd., Ann Arbor, MI 48105-1593.  
E-mail: lofgren@glerl.noaa.gov

cluded simulations of soil moisture, the length of their model runs was not sufficient to eliminate problems with dependence on initial conditions and signal to noise ratio in the output data sample. This study will concentrate on the soil moisture and use general circulation model (GCM) runs of at least 7 yr for greater confidence in the results.

The net effect of surface albedo perturbations on soil moisture may be dependent on latitude since Charney's argument that high surface albedo cools the overlying air and leads to sinking motion applies primarily to the low latitudes, where motion and precipitation are characterized by thermally direct motions. At midlatitudes, where the Coriolis factor is larger and atmospheric motion and precipitation are characterized by baroclinic waves, surface albedo's effect on precipitation may be much reduced, making its influence on potential evaporation more important at midlatitudes than at low latitudes.

The effects of surface albedo perturbations on thermal forcing of the atmosphere may be different if sea surface temperature is allowed to come into equilibrium with this perturbed forcing. Therefore, additional experiments have been performed using a slab mixed-layer representation of ocean thermodynamics.

Section 2 describes the GCM that was used in this study. Section 3 describes the experimental strategy. Results from experiments with globally prescribed perturbations in surface albedo will be shown in section 4. In section 5, latitude-dependent perturbations will be investigated, and in section 6, they will be combined with an ocean model whose surface temperature can respond to them. Conclusions are presented in section 7.

## 2. Model formulation

The model used for the simulations discussed in this paper is a version of the Geophysical Fluid Dynamics Laboratory (GFDL) GCM, which uses the spectral transform method to solve the equations of motion, the thermodynamical equation, and continuity equations of mass and moisture in order to compute the vertical component of vorticity, horizontal divergence, temperature, surface pressure, and water vapor mixing ratio. The version used here has a vertical resolution of nine unevenly spaced sigma layers and uses rhomboidal-15 horizontal resolution, which transforms to a grid of 7.5° longitude by 4.5° latitude. The main features of the dynamical component of this model are described in Gordon and Stern (1982).

These simulations have prescribed insolation at the top of the atmosphere, which varies seasonally but not diurnally. Except where noted, the sea surface temperatures were prescribed according to climatology. The calculations of atmospheric absorption and scattering of solar radiation are based on the scheme of Lacis and Hansen (1974), and the calculations of absorption and

emission of thermal longwave radiation use the scheme of Rodgers and Walsh (1966), as modified by Stone and Manabe (1968).

Large-scale precipitation is indicated by the model when the prognostic equation for water vapor yields a supersaturated value. This precipitation is identified as snow if the air temperature just above the surface is below 0°C, and as rain otherwise. Moist convection is handled by the moist convective adjustment scheme of Manabe et al. (1965). Clouds are predicted in the model using the scheme described in Wetherald and Manabe (1980), in which clouds are assumed to be present where relative humidity exceeds 99% or moist convection occurs.

The temperature of all land surfaces in the model is determined diagnostically by assuming that the input of solar energy is balanced exactly by the outputs of net outgoing longwave radiation, sensible heat flux, latent heat of evaporation or sublimation, and latent heat of snow- or icemelt.

The amount of evaporation or sublimation is given as the product of potential evaporation ( $E_p$ ) and  $\beta(w)$ , a function of soil moisture. The potential evaporation is given by

$$E_p = C_d \rho |\mathbf{v}(9)| [q_s(T^*) - q_9], \quad (1)$$

where  $C_d$  is the surface drag coefficient (taken as 0.003 over land, and 0.001 over ocean),  $\rho$  is the density of air at the surface,  $\mathbf{v}(9)$  is the wind velocity at the lowest model level (level 9, centered at  $\sigma = 0.99$ , or approximately 85 m from the surface),  $q_s(T^*)$  is the saturation mixing ratio given the potential temperature of the surface, and  $q_9$  is the water vapor mixing ratio of the atmosphere in the lowest model level. Term  $\beta$  is given by the expression

$$\beta = \frac{4}{3} \frac{w}{w_{fc}}, \quad \text{when } w < \frac{3}{4} w_{fc} \quad (2)$$

$$\beta = 1, \quad \text{when } w > \frac{3}{4} w_{fc}. \quad (3)$$

In this way, the bucket model reacts to moisture stress, although this formulation makes vegetation's resistance to evapotranspiration more implicit than some other parameterization schemes. For the experiments presented here, a field capacity ( $w_{fc}$ ) of 15 cm of water is assigned to all land areas.

Soil moisture is calculated using the bucket model described in Manabe (1969). The prognostic equation for soil moisture is

$$\frac{\partial w}{\partial t} = R + S - E - F, \quad (4)$$

where  $R$  is rainfall,  $S$  is snowmelt,  $E$  is evaporation, and  $F$  is runoff. Runoff is indicated only when the soil moisture exceeds the field capacity (15 cm in most sim-

ulations herein), in which case the excess is treated as runoff.

Note that in order to maintain the surface energy balance, the surface temperature rises when the soil moisture and evaporation are low. Because of this, the value of  $E_p$  is sensitive to the soil moisture. This is discussed in Milly (1992), where it is shown that the definition of  $E_p$  in (1) is distinct from the more traditional definition of  $E_p$ , in which  $q_s(T^*)$  is calculated by using the lower temperature of a hypothetically saturated surface rather than the higher temperature of a surface with limited soil moisture. This distinction causes the model-predicted soil moisture to be lower when using this model's definition of  $E_p$  rather than the traditional definition. All of the model simulations discussed here use the same definition of  $E_p$ , but because the  $E_p$  values are excessively high for dry surfaces, the response in soil moisture to a change in precipitation is amplified. Nevertheless, the model's soil moisture can be considered, with the above caveats, to be a qualitative gauge of a region's wetness when comparing the simulations discussed here.

For the control case, the albedo of land not covered by snow is prescribed to the modern values (constant throughout the seasonal cycle) given in the CLIMAP (1981) dataset, in which surface albedos are assigned based on data on the global distribution of surface types combined with the corresponding albedos given by Kukla and Robinson (1980).

Increased values of surface albedo are predicted where snow is present. Thick snow (greater than 2 cm water equivalent depth) is assigned albedo from 0.45 to 0.6 depending on temperature, with reduction for lesser snow depth. Glaciated grid points are assigned surface albedos between 0.55 and 0.80, depending on temperature and snow cover.

Most of the simulations used in this study use prescribed sea surface temperatures, but those described in section 6 use sea surface temperature predicted by assuming a mixed layer at the surface of the ocean. For equilibrium cases such as those considered here, this is a computationally economical alternative to a full dynamical ocean model. The sea surface temperature was prognostically determined using the equation

$$C \frac{\partial T}{\partial t} = SR - LR - SH - LE + Q, \quad (5)$$

where  $C$  is the heat capacity appropriate for a mixed layer 50 m deep,  $SR$  is the net incoming solar radiation,  $LR$  is the net outgoing longwave radiation,  $SH$  is the sensible heat flux, and  $LE$  is the latent heat flux. Term  $Q$ , known as the  $q$ -flux, is a flux from the bottom of the mixed layer, assumed to be due to oceanic heat transport, which is prescribed such that the control case does not drift from observed sea surface temperatures despite an imbalance among the fluxes of radiative, sensible, and latent heat. There is also a component of

the model that predicts sea ice cover. To prevent growth of the sea ice volume without bound, limits are enforced by the model on its thickness, but its areal extent is not constrained.

It is acknowledged that some of the physical parameterizations used here, particularly the moist convective adjustment scheme (see discussion in Frank and Molinari 1993) and the bucket model of soil moisture, are simple compared with those used in other models. However, they have the advantage of being free from excessive tuning, and the single bucket model is able to summarize the hydrologic state of the surface using only one parameter, the soil moisture.

### 3. Experimental strategy

In order to investigate the sensitivity of soil moisture to surface albedo perturbations at different latitudes individually and to distinguish between local effects and remotely caused effects, experiments were carried out with perturbations to surface albedo over the entire globe and over individual latitude belts: 1) the extratropical belt, where the time-mean vertical motion is weak and precipitation is associated with transient eddies that arise due to baroclinic instability, 2) the subtropical belt, where rainfall is often suppressed due to the downward motion of the Hadley cell, although some portions have strong seasonal (monsoon) rainfall, and 3) the tropical belt, which contains the upward branch of the Hadley cell and some of the areas of highest annual precipitation.

A summary of the GCM simulations is included in Table 1. A control case was run using the CLIMAP distribution of surface albedo (Fig. 1) for a 15-yr simulation, following a 2-yr spinup period; several experimental cases with prescribed perturbations to land surface albedo were each run for 7 yr after the initial spinup. In all cases, the prescribed value of surface albedo

TABLE 1. Prescribed surface albedo runs (at R15 resolution). See Fig. 1 for outlines of experiment domains.

	Sea surface temperature	Land-surface albedo perturbation	Perturbed domain
R15 control	prescribed	none	
GI	prescribed	+0.10	global
GD	prescribed	-0.10	global
EI	prescribed	+0.10	>31°, both hemispheres
ED	prescribed	-0.10	>31°, both hemispheres
SI	prescribed	+0.10	9°-31°, both hemispheres
SD	prescribed	-0.10	9°-31°, both hemispheres
TI	prescribed	+0.10	9°S-9°N
TD	prescribed	-0.10	9°S-9°N
ConMO	mixed layer	none	
GIMO	mixed layer	+0.05	global
G15	prescribed	+0.05	global

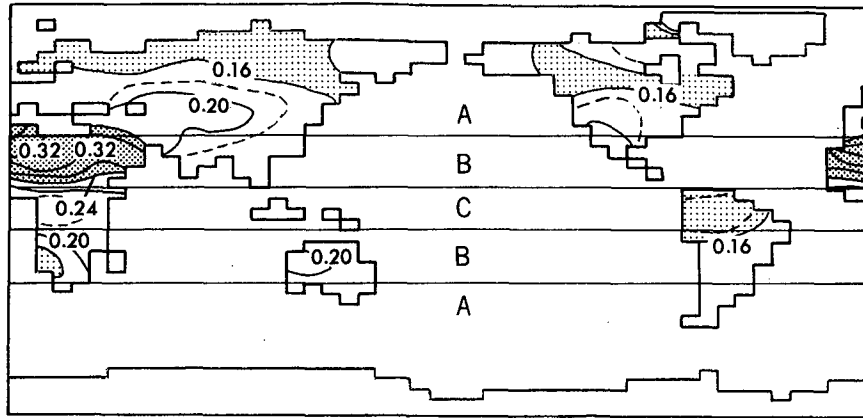


FIG. 1. Distribution of snow-free land surface albedo used for the control run (derived from CLIMAP 1981). The solid contours are at intervals of 0.04, and the dashed contours represent 0.14 and 0.18. These surface albedos are altered in the presence of snow using the parameterization described in section 2. Also shown are the boundaries between the latitude belts over which surface albedo was altered in the latitude belt experiments.

was altered for the presence of snow using the parameterization described in section 2. In the first two experiments, global increase (GI) and global decrease (GD), the surface albedo (in the absence of snow) is increased and decreased, respectively, by 0.10 over all nonglaciated land surfaces. In the extratropical increase (EI) and extratropical decrease (ED) experiments, snow-free surface albedo perturbations of 0.10 are applied only to nonglaciated land points in the area indicated by the letter A in Fig. 1. In the subtropical increase (SI) and subtropical decrease (SD) experiments, surface albedo is perturbed on land in area B in Fig. 1. In the tropical increase (TI) and tropical decrease (TD) experiments, surface albedo is perturbed on land in area C in Fig. 1. All of these experiments have sea surface temperature prescribed according to climatology. Using opposite perturbations in surface parameters allows greater confidence that a diagnostic

quantity (precipitation, for example) is sensitive to that parameter if that quantity has changes from the control case of opposite sign in the two perturbed cases. It also gives an indication of linearity or nonlinearity of the response.

In analyzing the results of this series of experiments, it was advantageous to subdivide the portion of northern Africa in the subtropical belt to examine the heat and water budgets of the surface and the heat budget of the atmosphere. Thus, this paper will present the difference in response between the region referred to as the Sahel, which is moist during the summer rainy season, and the Sahara, which is dry throughout the year. These regions are labeled 1 and 2, respectively, in Fig. 2.

In addition to examining the responses to surface albedo perturbations in the presence of prescribed sea surface temperature, it should be determined whether

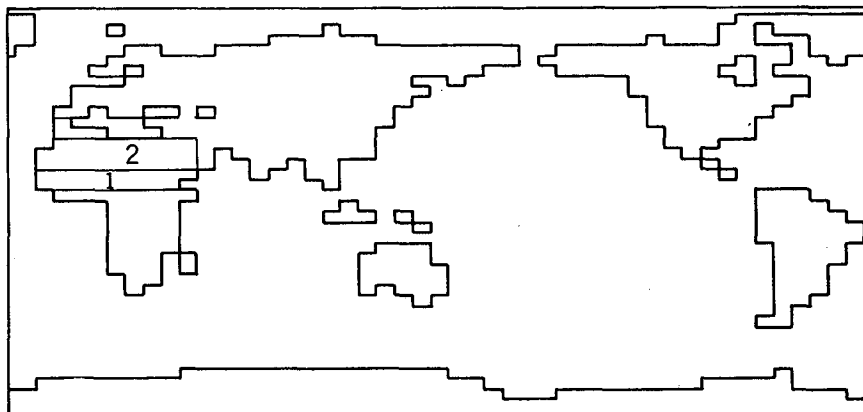


FIG. 2. Location of regions referred to for areal averages in following figures.

model responses are similar when sea surface temperature responses are included through a mixed-layer ocean formulation. A change in heating of air over the continents can be passed to the ocean by advection. In this case, the forcing of atmospheric motion and precipitation may be different from the case with prescribed sea surface temperatures. Using the mixed-layer ocean formulation along with increased surface albedo can also be considered a simple analog for the cooling influence of lower tropospheric aerosols, which can affect temperature beyond the aerosol's location due to advection. Charlson et al. (1992) report on cooling at the surface by sulfate aerosols from the combustion of fossil fuels. This aerosol is concentrated over and downwind from industrial areas, primarily in and near the continents of the Northern Hemisphere. Penner et al. (1992) suggest similar effects due to carbon-based aerosol in the lower troposphere from the burning of biomass.

Therefore, another control case was run using the mixed-layer ocean formulation given in (7), in which the surface albedo was given the values from CLIMAP (1981). This will be called the control case with mixed-layer ocean, or ConMO (Table 1). The experimental case, referred to as the increased surface albedo case with mixed-layer ocean, or GIMO (Table 1), has surface albedo globally increased by only 0.05 in order to reduce the incidence of reaching the maximum sea ice thickness in the GIMO case. For direct comparison to GIMO, another experiment with prescribed sea surface temperature was run with land surface albedo globally increased by 0.05. This is called GI5 (Table 1). The distribution of  $q$ -flux over the oceans (see section 2) is the same in the ConMO and GIMO cases, implying identical horizontal heat transport by the oceans.

#### 4. Control case and global perturbations

Because the bulk of the world's nonglaciated land is located in the Northern Hemisphere, the strongest effects of perturbing the land surface albedo occur during the Northern Hemisphere summer, when the solar forcing there is greatest and most of the land is snow-free. (Snow-covered areas are not affected by the prescribed surface albedo perturbations since their surface albedo is parameterized according to the snow depth.) For this reason, most of the data presented in this paper will consist of mean values for the months of June, July, and August (JJA).

Figure 3 shows the model's mean precipitation during JJA and compares it with observed precipitation for the same 3-month period. Several figures in this paper, including Fig. 3a, use spatial smoothing to extract information at spatial scales larger than the scale of smoothing, without the distraction of computational noise at the scale of finest resolution. Precipitation is a particularly noisy field, with time-averaged values on

adjacent grid boxes differing by factors up to approximately 2, especially in the vicinity of isolated topographic features. In both the observations and the model, the highest concentrations of precipitation over land are in Central America and northern South America, a belt across Africa centered at about  $10^{\circ}\text{N}$ , and southern Asia. In comparison with observations, the model's precipitation is light over central Africa, Central America, and northern South America, and the area of heavy precipitation in southern Asia is shifted toward Indochina, reducing precipitation in India.

There are large areas of low precipitation in the subtropics, but these areas are not as large nor as dry in the model as in the observations, especially in southern Africa, Australia, and the Gobi Desert of eastern Asia, where a strong precipitation minimum is absent in the model.

In both the observations and the model, there is a strong band of precipitation over the ocean in the Pacific intertropical convergence zone (ITCZ), just north of the equator. A weaker ITCZ also appears in the Atlantic. Precipitation is also relatively heavy between  $30^{\circ}$  and  $40^{\circ}\text{S}$ , as well as on and near the eastern coasts of North America and Asia.

A direct effect of changing the surface albedo is to change the surface temperature and the air temperature. Figure 4 shows the responses of surface air temperature during JJA to an increase and decrease in surface albedo over all land. With increased surface albedo (Fig. 4a), surface air temperature is decreased over nearly all land, with most parts of the Northern Hemisphere midlatitudes having a  $2^{\circ}$ – $5^{\circ}\text{C}$  decrease. The exception is in Africa, just north of the equator, where precipitation and soil moisture are significantly decreased. This limits latent heat flux and enhances sensible heat flux, which warms the near-surface air. Because the sea surface temperature is the same in both cases, the changes in air temperature just above the oceans are small. The results from decreased surface albedo (Fig. 4b) are qualitatively opposite. Surface air temperatures over the Northern Hemisphere midlatitudes are increased by  $2^{\circ}$ – $5^{\circ}\text{C}$ , temperature is decreased in Africa just north of the equator, and temperature changes over the oceans are near zero.

Figure 5 shows the changes in JJA precipitation due to globally increased and decreased land surface albedo. The largest changes in precipitation occur in the low-latitude land areas where the control case has its heaviest precipitation during this season. In experiment GI (Fig. 5a), precipitation is decreased in most of Africa, southern Asia, and large portions of South America, by amounts up to about  $3.5\text{ mm day}^{-1}$ . In experiment GD (Fig. 5b), precipitation is increased in central Africa, southern Asia, and most of South America. However, precipitation perturbations over Central America are of opposite sign to those in other tropical and subtropical rainbelts, an extension of the response over the Atlantic.

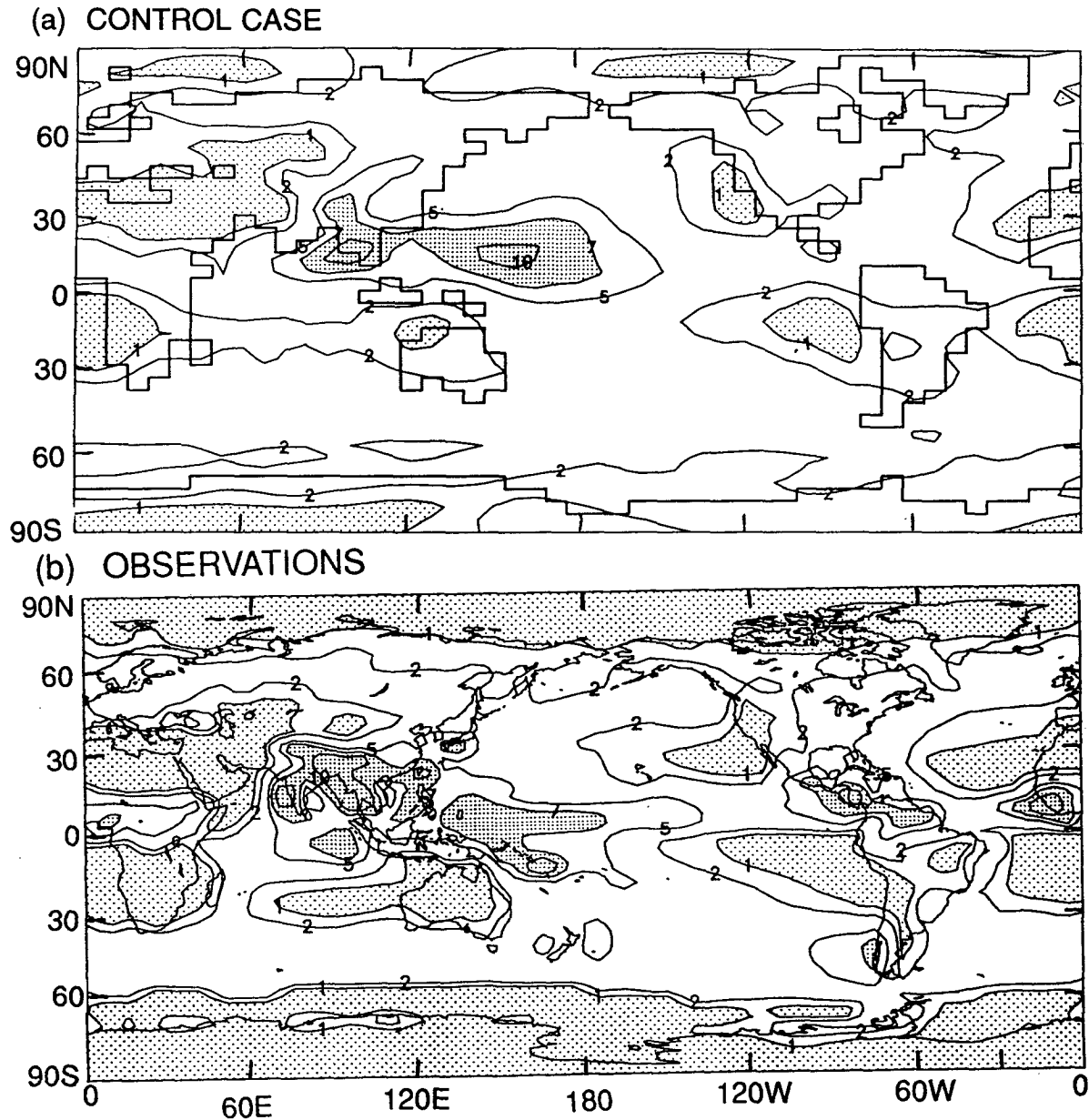


FIG. 3. June, July, and August precipitation for (a) the control case, and (b) the observations of Jaeger (1976), in units of millimeters per day. Heavy shading indicates values greater than  $7 \text{ mm day}^{-1}$ , light shading less than  $1 \text{ mm day}^{-1}$ . To suppress noise at the grid scale, a 1–2–1 spatial smoothing has been applied.

In GI, precipitation increases over much of North America, Europe, and western Asia. Although some of these increases are statistically significant, their amplitude is smaller than those at low latitudes. Eastern Asia has decreased precipitation in both GI and GD.

Figure 6 shows the changes in soil moisture that result from global surface albedo perturbations. In GI, the strong decreases in precipitation over the low-latitude rainbelts—central Africa, southern Asia, and northern South America—result in decreased soil moisture, but there is not such a consistent change in

soil moisture in other parts of the low latitudes, such as the Sahara and Australia. Soil moisture is almost invariably increased in the midlatitudes of the Northern Hemisphere. Correspondingly, in GD soil moisture is increased in central Africa, southern Asia, and northern South America but is decreased throughout the midlatitudes of the Northern Hemisphere and has little change in low-latitude regions outside of the rainbelts.

The global experiments point out that there is a qualitative difference in the response among the latitudes. Tropical rainbelts have large systematic changes in pre-

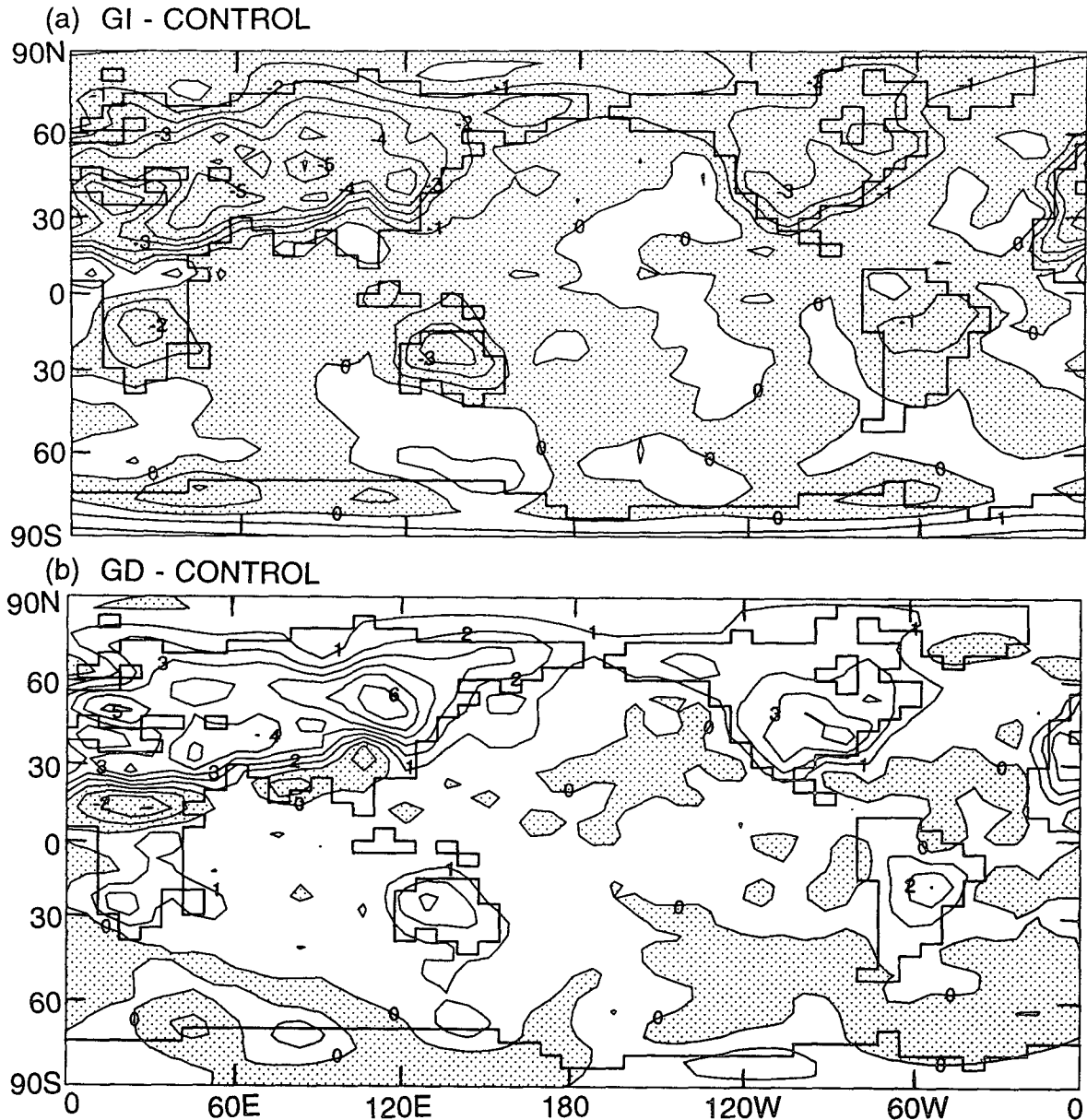


FIG. 4. June, July, and August surface air temperature for (a) GI minus control and (b) GD minus control. The contour interval is 1°C. Shading indicates a decrease. Smoothing is as in Fig. 3.

precipitation and soil moisture and perhaps counterintuitive changes in air temperature. Subtropical arid regions have smaller responses in precipitation and soil moisture. Midlatitude regions have small changes in precipitation, but systematic changes in soil moisture of opposite sign to those in the low-latitude rainbelts. The following section will describe and explain differences in response between the low latitudes and the midlatitudes in the model, using the experimental cases in which surface albedo was changed over individual latitude belts.

## 5. Experiments on individual latitude belts

### a. Subtropical experiments

Figure 7 shows the zonal mean over land of the differences during JJA between the subtropical experiments and the control case for precipitation, vertical velocity (in pressure coordinates) at 515 mb, evaporation, potential evaporation, and soil moisture. For convenience in comparing the experiments with opposite perturbations to the surface albedo, Fig. 7 shows these quantities for SI minus control and control minus

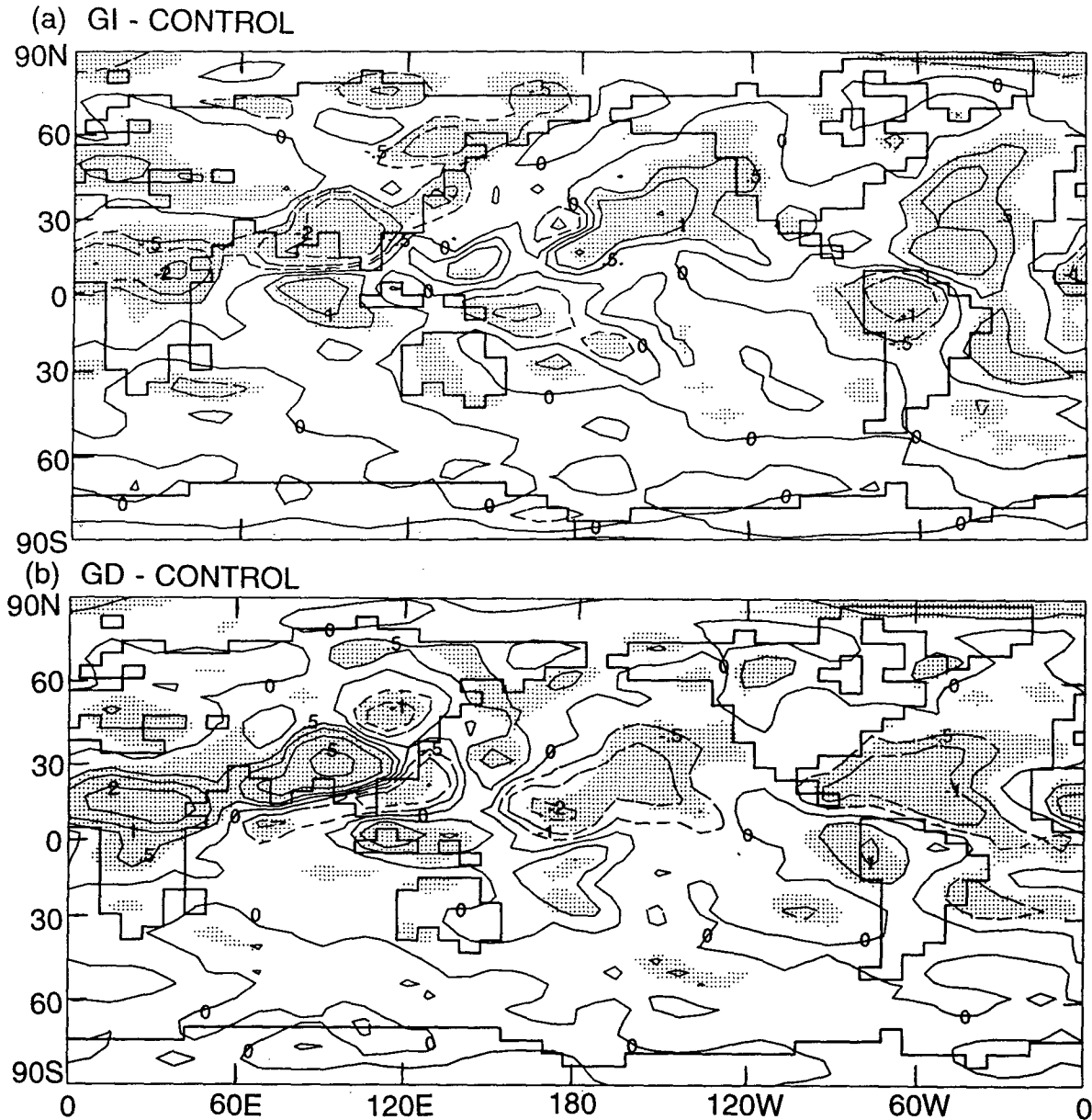


FIG. 5. June, July, and August precipitation for (a) GI minus control and (b) GD minus control. Contours represent 0,  $\pm 0.5$ , 1, 2, and 5  $\text{mm day}^{-1}$ , with dashed contours for negative values. Regions with precipitation changes significant at the 95% level or greater are shaded. Smoothing is as in Fig. 3.

SD. A precisely linear response in any quantity with respect to changes in surface albedo will result in identical curves.

The precipitation response to subtropical perturbations in surface albedo during JJA (Fig. 7a) is greater in the subtropics of the Northern (summer) Hemisphere than in the Southern Hemisphere, with the strongest response in the SI case being near the southern edge of the Northern Hemisphere subtropical belt (corresponding to the West African monsoon region). In the Northern

Hemisphere subtropical belt, SI consistently shows a decrease in zonal mean precipitation over land. SD shows an increase, but in the southern portions of the subtropical belt it is smaller than the decrease in SI.

In the Northern Hemisphere Tropics and subtropics, the changes in precipitation are well correlated with changes in vertical velocity at 515 mb ( $\omega$ , in pressure coordinates, Fig. 7b). Here SI has an increase in  $\omega$  in the Northern Hemisphere subtropics, where precipitation is decreased. Outside of the range of approximately

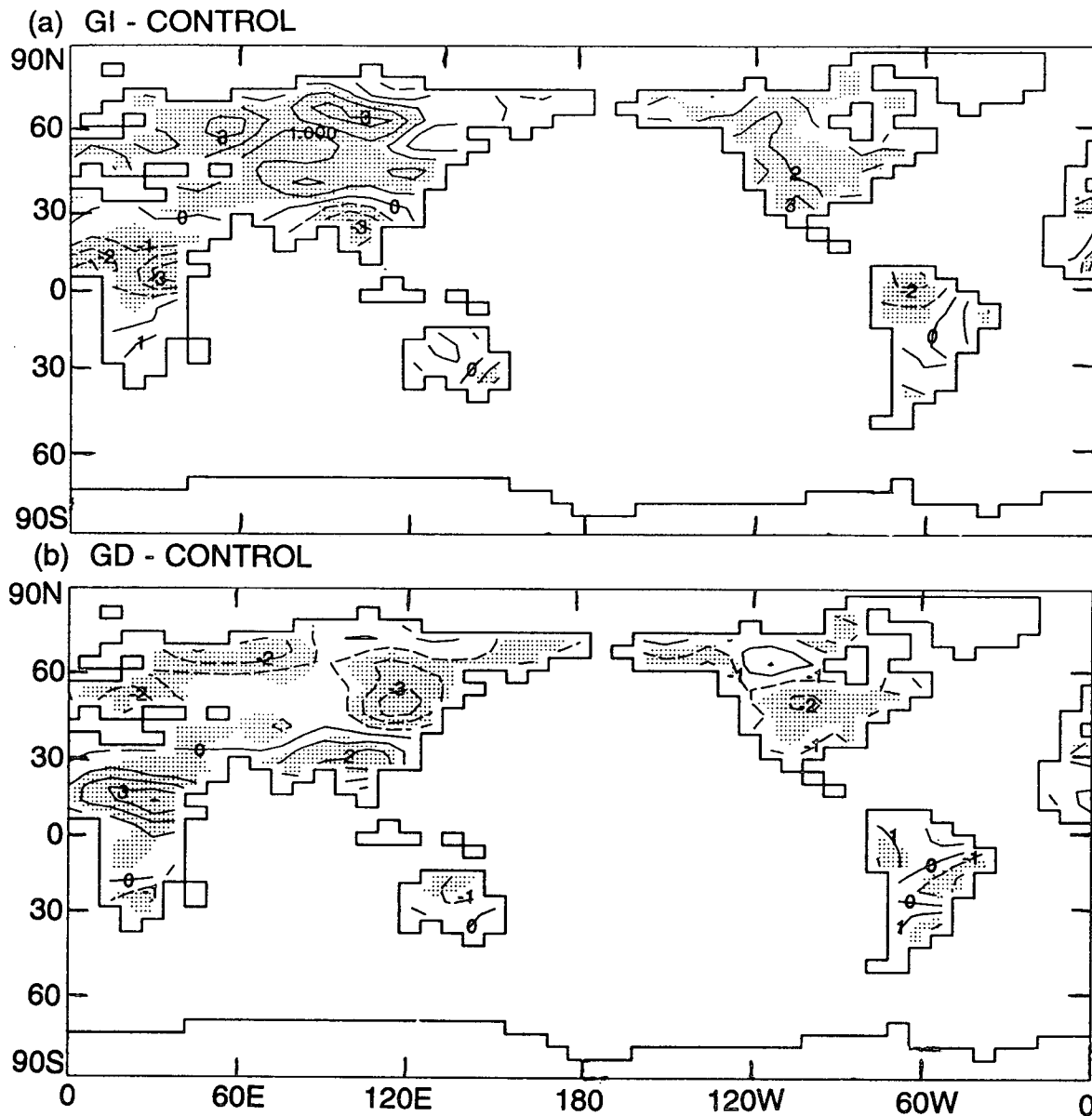


FIG. 6. June, July, and August soil moisture for (a) GI minus control and (b) GD minus control. The contour interval is 1 cm, with dashed contours for negative values. Regions with soil moisture changes significant at the 95% level or greater are shaded. Smoothing is as in Fig. 3.

0°–31°N, there is not a clear correlation between responses in precipitation and in  $\omega$ .

The changes in evaporation (Fig. 7c) qualitatively follow the changes in precipitation, being decreased in SI and increased in SD in the Northern Hemisphere subtropics. In the monsoonal regions, where the largest changes in precipitation occur, the change in evaporation is considerably smaller than the change in precipitation, with the difference being associated with relative water vapor flux divergence in the air and decreased runoff on the ground.

Potential evaporation (Fig. 7d) is generally decreased in experiment SI because more solar radiation is reflected from the surface, less radiative energy is available for evaporation, and the surface temperature drops. The greatest decrease in potential evaporation is in the dry subtropics of the summer (Northern) hemisphere. As mentioned in conjunction with (1), the value of potential evaporation and the amplitude of changes in it are exaggerated, especially in arid regions. Note the difference in scale of Fig. 7d in comparison to Figs. 7a and 7c.

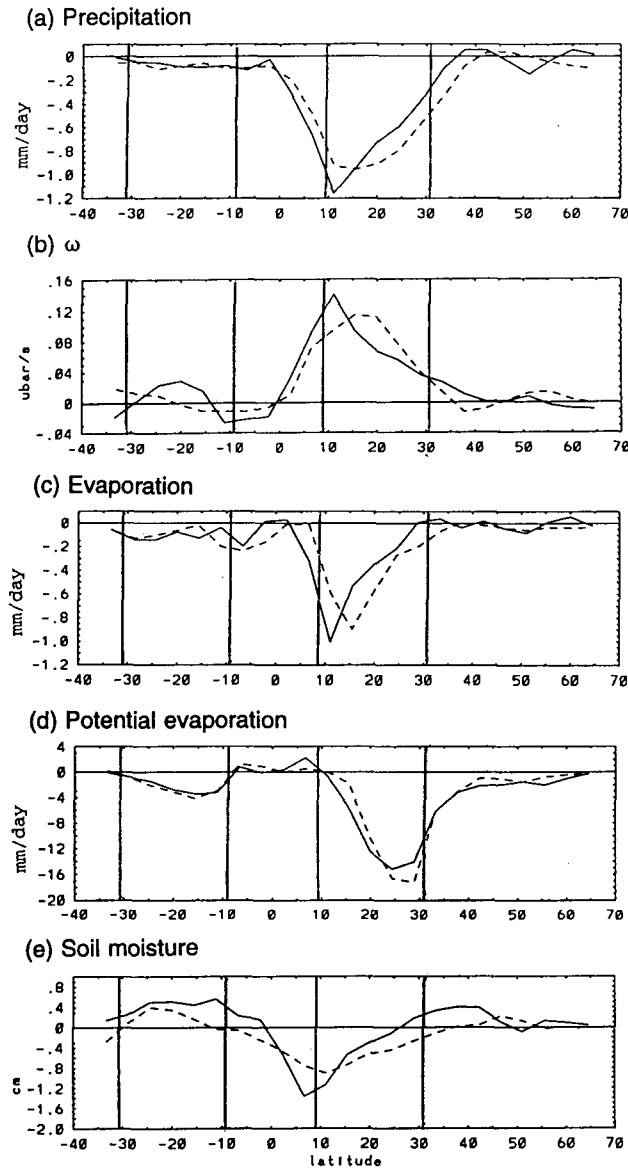


FIG. 7. Zonal means over land only for SI minus control (solid curve) and control minus SD (dashed curve) during June, July, and August of (a) precipitation, (b) vertical velocity at 515 mb in pressure coordinates, (c) evaporation, (d) potential evaporation, and (e) soil moisture. Vertical lines indicate the boundaries of the latitude belts affected by surface albedo perturbations. Latitude circles with fewer than four nonglaciated land points are not displayed.

Soil moisture (Fig. 7e) responds in the same sense as precipitation (Fig. 7a) in the subtropics. The size of soil moisture responses is also partially controlled by the potential evaporation and runoff. The geographical distribution of changes in soil moisture during JJA due to the perturbation of surface albedo in the subtropics alone (not shown) are similar to those in the subtropics in the experimental cases with global perturbations of surface albedo (Fig. 6). In the region of the south Asian

monsoon (near 25°N), soil moisture is little influenced by precipitation changes, with precipitation changes being directly reflected in runoff, rather than significantly affecting evaporation or soil moisture. Also, the changes in soil moisture in the Sahara (also in the vicinity of 25°N) are modest.

The JJA precipitation responses to surface albedo perturbations in the subtropical belt (Fig. 8) are similar to those noted in the subtropics due to global perturbations (Fig. 5). That is, in SI, summertime precipitation is reduced over northern Africa and southern Asia, and in SD, precipitation is increased in the same areas. Precipitation responses are particularly strong over a small area in Indochina, where the GCM predicts the maximum rainfall of the Asian summer monsoon (Fig. 4). In this region, SI shows a decrease of as much as 4 mm day<sup>-1</sup> (about 50% of the control case precipitation), and SD an increase of up to 9 mm day<sup>-1</sup> (more than 100%).

#### 1) SAHEL

It must now be determined what mechanisms produce the noted changes in circulation, precipitation, and soil moisture. These must ultimately be linked to radiative forcing due to perturbed surface albedo and the way in which it alters the surface heat balance and atmospheric diabatic heating. Since it was noted that the magnitude of the response in terms of precipitation during the summer is very different between the regions that ordinarily have heavy summer (monsoon) rainfall and those that are dry for the entire year, regions representative of each of these cases have been chosen for further analysis. Figure 2 shows these as regions 1 and 2.

Region 1, the Sahel, is the portion of Africa between 9° and 18°N. This is a region of grassland and savanna and is dry during the winter and rainy during the summer. By decreasing the surface albedo, precipitation during JJA in the Sahel is increased by a mean of 1.5 mm day<sup>-1</sup> (from 2.6 mm day<sup>-1</sup> in the control case), and soil moisture is increased by 1.8 cm (from 2.7 cm in the control case).

The change in thermal forcing of the atmosphere in this region caused by surface albedo perturbations is initially due to changes in the latent plus sensible heat flux from the surface, which is equal to the net radiative heating of the surface (which is increased by 18.1 W m<sup>-2</sup>). Because the soil in this region is moistened and cooled during the summer in case SD, sensible heat flux is reduced by an average of 6.6 W m<sup>-2</sup> during JJA. However, latent heat flux is increased by 24.7 W m<sup>-2</sup>.

This enhanced latent heat flux can contribute to local diabatic heating through release in convective activity near its point of origin; however, it also feeds back on itself. Figure 9 shows the vertical distribution of change in heating due to boundary-layer diffusion, radiative flux convergence, and convection resulting from a de-

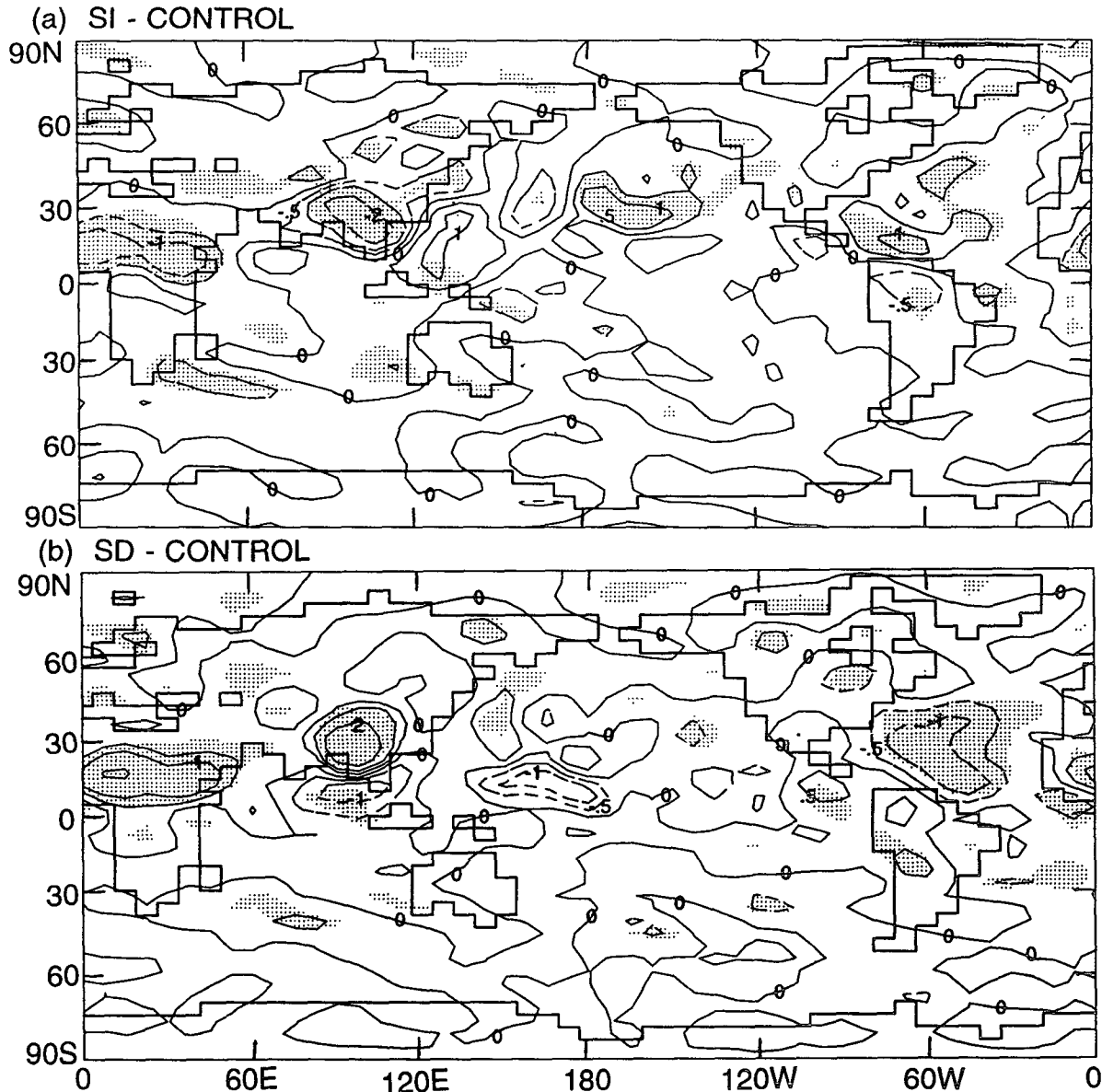


FIG. 8. As in Fig. 5 except for (a) SI minus control and (b) SD minus control.

crease in surface albedo during JJA, averaged over the Sahel. The convection term shown is the sum of heating due to latent heat release by convective condensation and vertical heat exchange by moist and dry convection. From Fig. 9 it can be seen that there is a modest increase in radiative heating in the middle and upper troposphere. The noted reduction in sensible heat flux is evidenced in relative cooling at the lowest levels by boundary-layer diffusion.

The largest impact is in the convection term. The vertical exchanges of heat due to convective motion simply move heat from one layer to another, so their vertical sum is zero. The vertical integral of convective

heating, which is increased by an average of  $67.2 \text{ W m}^{-2}$  in case SD, is thus strictly due to latent heat release. This is considerably larger than the  $24.7 \text{ W m}^{-2}$  increase in latent heat flux from the ground, with the difference being provided by the convergence of water vapor flux. Convective heating is strongest in the mid-troposphere, although it should be noted that the lower layers contain less mass than the midlayers ( $\Delta\sigma$  for level 9 is only 0.02, while for level 5 it is 0.17), so equivalent changes in latent heat release would have a larger effect on temperature there.

Thus the increased heat flux from the local surface adds heat to the overlying atmosphere, and this heating is en-

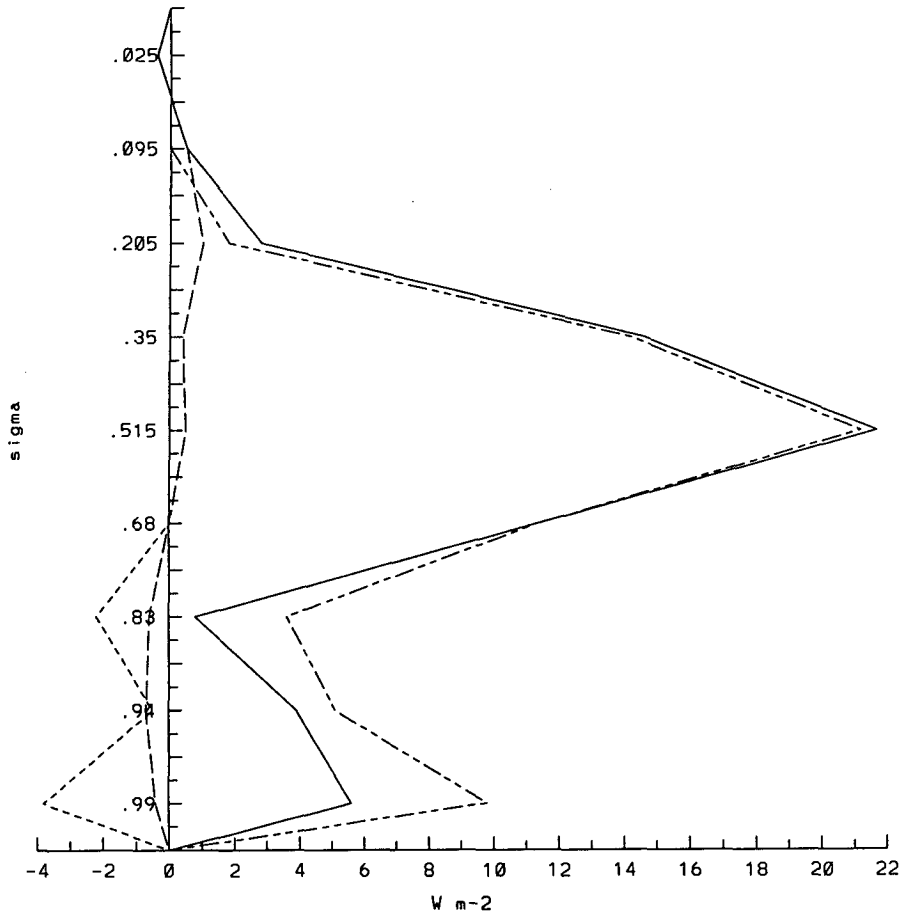


FIG. 9. Total diabatic heating (solid line, column total is  $52.7 \text{ W m}^{-2}$ ) and its components due to vertical diffusion (dotted line, column total is  $-4.8 \text{ W m}^{-2}$ ), radiation (dashed line, column total is  $5.9 \text{ W m}^{-2}$ ), and convection (dash-dotted line, column total is  $51.6 \text{ W m}^{-2}$ ), averaged over the Sahel (region 1 in Fig. 2), for experiment SD minus control during June, July, and August. The model's unequally spaced sigma levels are displayed with equal spacing in the figure, so that the area to the left of the curve is the total column heating.

hanced by a positive feedback mechanism. In accordance with Held (1985), the depth of heating due to latent heat released in deep convection, along with its location at a low latitude, means that it is mainly balanced by adiabatic cooling and upward motion. This upward motion requires the convergence of moist air at low levels and the divergence of dry air aloft, and so involves significant net convergence of water vapor flux, further increasing both latent heat release and precipitation.

In contrast to what might be expected when prescribing a change in surface albedo, the change in net radiative heating of the surface in the Sahel during JJA is not primarily due to solar heating. The solar absorption is increased in SD by a modest  $7.8 \text{ W m}^{-2}$ , or 3.6% of the control case value, because of increased cloudiness. However, the clouds also trap and reradiate longwave radiation, so that the net outgoing longwave radiation in the Sahel is decreased by  $17.3 \text{ W m}^{-2}$  in SD, or 17.6% of the control case value, for a net increase

of  $25.1 \text{ W m}^{-2}$ , which approximates the increase of  $25 \text{ W m}^{-2}$  expected from multiplying the net incoming solar radiation by the change in surface albedo. The net effect of the change in cloudiness, in comparison with a case with constant cloudiness, has not been evaluated.

Large responses in precipitation and soil moisture in the Sahel are limited to the summer. During the winter, this region's soil is dry, and water vapor from the oceans goes toward the tropical rainbelt far to the south. Therefore, this region has little opportunity to increase its rainfall either through increased local evaporation or through increased water vapor flux convergence. Soil moisture is also little changed during the winter.

Increased surface albedo in the Sahel (not shown) produces results qualitatively opposite to decreased surface albedo. Diabatic heating is decreased over a great depth of the atmosphere during the summer, as is water vapor flux convergence. Rainfall and soil moisture are reduced during the summer to less

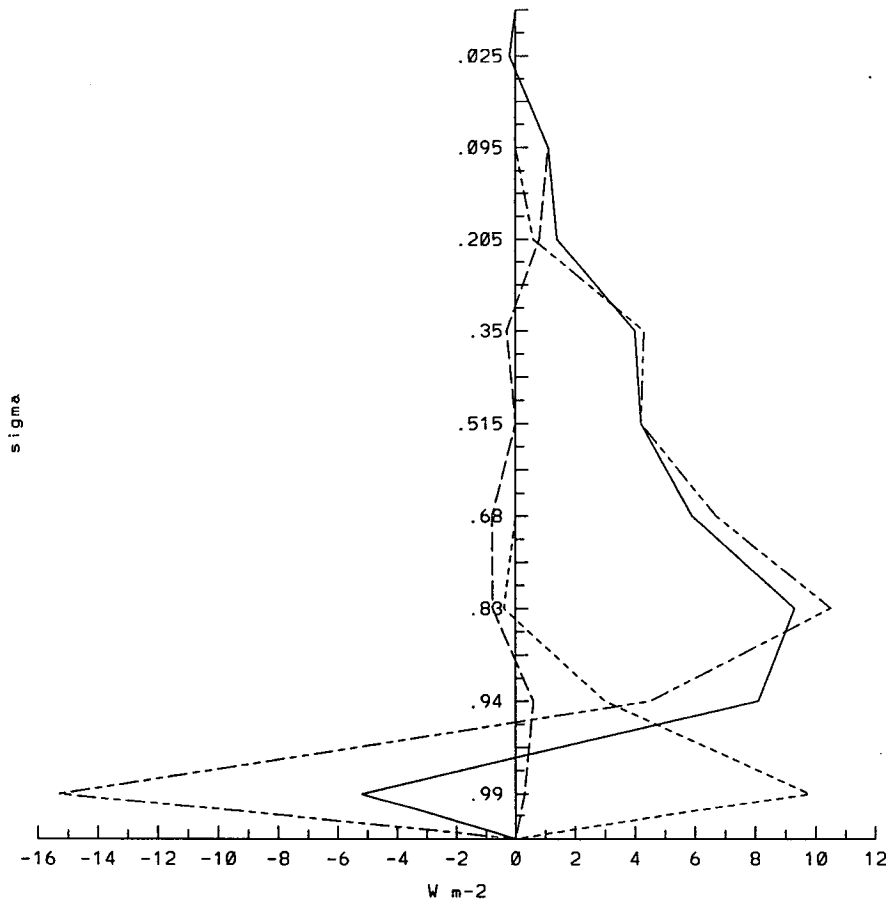


FIG. 10. As in Fig. 9, except for the Sahara (region 2 in Fig. 2). The change in total diabatic heating is  $33.5 \text{ W m}^{-2}$ , total vertical diffusion— $19.3 \text{ W m}^{-2}$ , total radiative heating— $3.3 \text{ W m}^{-2}$ , and total convective heating— $10.9 \text{ W m}^{-2}$ .

than one-third of their control case values during August.

## 2) SAHARA

The region referred to as the Sahara is the portion of Africa lying between  $18^\circ$  and  $31^\circ\text{N}$  latitude (region 2 in Fig. 2). This part of Africa is dry all year. The changes in diabatic heating due to reduced surface albedo over the Sahara during JJA are shown in Fig. 10. As in the Sahel, there is an increase in diabatic heating, but it is mainly due to vertical diffusion (sensible heat flux) in the lower troposphere. Much of the sensible heat deposited in the boundary layer is transported upward by convection (primarily dry convection in this region). The column's increase in latent heat release is  $15.4 \text{ W m}^{-2}$ , while the local latent heat flux is increased by  $9.8 \text{ W m}^{-2}$ . This indicates that condensation in this region is enhanced by much less than in the Sahel, both because of a smaller increase in local evaporation (equivalent to  $24.7 \text{ W m}^{-2}$  in the Sahel, compared to  $9.8 \text{ W m}^{-2}$  in the Sahara) and because of a much

smaller increase in convergence of water vapor flux (equivalent to  $42.5 \text{ W m}^{-2}$  in the Sahel, compared to  $5.6 \text{ W m}^{-2}$  in the Sahara).

Although the absolute value of the increase in precipitation during JJA over the Sahara ( $0.6 \text{ mm day}^{-1}$ ) is less than that in the Sahel, it is nearly half of the precipitation in the control case ( $1.3 \text{ mm day}^{-1}$ ). The JJA soil moisture increase of  $0.4 \text{ cm}$  is as large as its mean value in the control case,  $0.4 \text{ cm}$ . In the SI case, summer precipitation over the Sahara decreases by  $0.4 \text{ mm day}^{-1}$ , and soil moisture decreases by  $0.1 \text{ cm}$ , a nonlinearity when compared with the larger responses of the SD case.

During the winter, precipitation in the Sahara is little affected by surface albedo perturbations, but soil moisture does respond. Because surface temperature and potential evaporation are increased in case SD, the soil moisture decreases to a lower level before evaporation comes into balance with precipitation. The annual mean soil moisture, however, is slightly increased. Here SI has soil moisture increased during the winter by a sufficient amount that its annual mean soil mois-

ture is also increased. This is another example of non-linearity between the two opposite experimental cases.

### b. Tropical experiments

In the rainy regions of the Tropics, such as equatorial Africa and the Amazon Basin, the responses in net radiative heating of the ground, diabatic heating of the atmosphere, precipitation, and soil moisture are qualitatively similar to those noted during the summer in the Sahel. That is, decreased surface albedo results in increased rainfall (from both increased local evaporation and increased water vapor flux convergence) and increased soil moisture. These responses occur all year but are particularly strong during the spring and fall, when the rainbelt is centered over these tropical regions. The solar absorption response to decreased surface albedo is small because of changes in cloudiness, but the decrease in net outgoing longwave radiation is such that there is always increased net radiative heating of the ground. There is also increased latent heat flux and decreased sensible heat flux.

In the zonal mean during JJA (Fig. 11), the maximum response in precipitation to tropical surface albedo perturbation occurs just north of the equator. Here TD has increased zonal mean precipitation over land throughout the Tropics, while TI has decreased precipitation. There is also a spillover effect on the latitude row of 11°N, where precipitation is decreased in TI and increased in TD despite the absence of a prescribed change in surface albedo at this location. Potential evaporation is changed little in both TI and TD because of the opposing effects of surface albedo and rainfall on the surface temperature and potential evaporation, but evaporation and soil moisture each have responses in concert with the change in precipitation. It should be noted that soil moisture changes by a larger amount in TI than in TD, reflecting the tendency of the ground in the Tropics to become saturated more often in TD, which prevents further increase in soil moisture.

### c. Extratropical experiments

During the summer, the continents of the midlatitude Northern Hemisphere, due to their relative inability to store heat, pass more heat to the overlying atmosphere than do the neighboring oceans. This heating is mostly offset by the cold advection from equatorward surface winds (not shown) over the midlatitude continents, as predicted by Held's (1985) linear quasigeostrophic model, and poleward flow off the east coasts of the continents. Decreasing (increasing) the land surface albedo strengthens (weakens) these winds but does not result in much time-mean convergence or divergence, either of wind flow or of water vapor flux. This tendency for advective rather than adiabatic cooling is partially attributable to the higher Coriolis parameter and is further promoted by the shallowness of the profile of

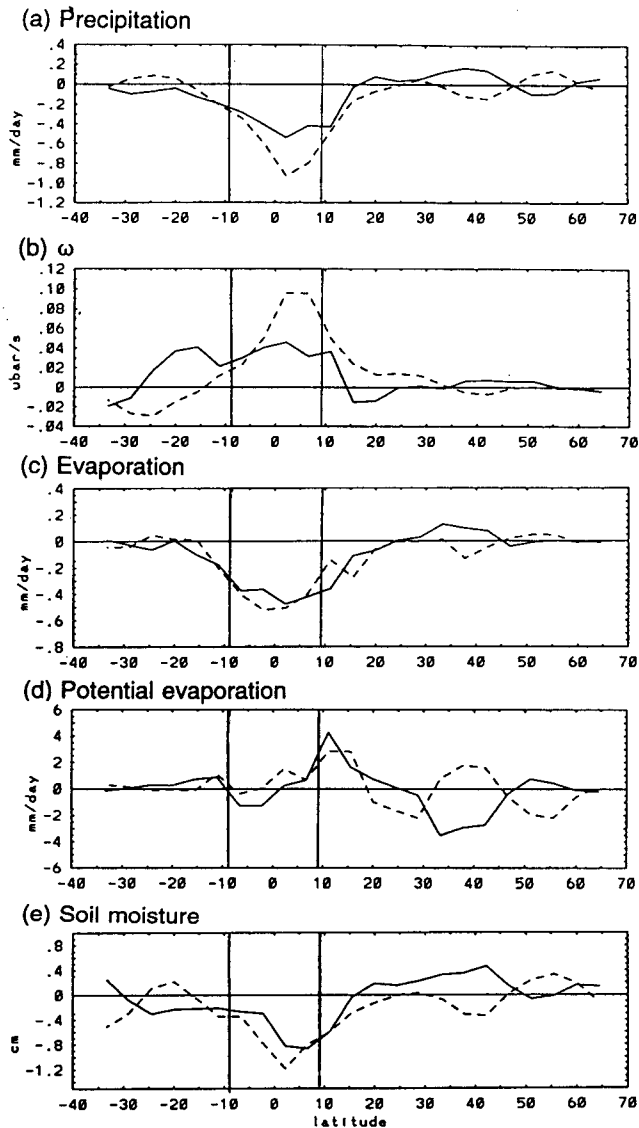


FIG. 11. As in Fig. 7 except the solid curves indicate TI minus control, and the dashed curves indicate control minus TD.

change in diabatic heating (not shown), which is due primarily to changes in sensible heat flux.

Outside of southern Asia, precipitation changes on land for experiments EI and ED (Fig. 12) are small in comparison to those induced by surface albedo perturbations in the Tropics and subtropics. However, Europe and western Asia are dominated by increases in precipitation in cases GI and EI and by decreases in precipitation in cases GD and ED. This also appears in the zonal mean precipitation change for JJA, shown in Fig. 13a. Between 38° and 47°N, EI has a modest increase in precipitation and ED a decrease during JJA. These changes in precipitation are not associated with changes in the vertical  $p$ -velocity (Fig. 13b), in contrast with the precipitation changes in the tropical and

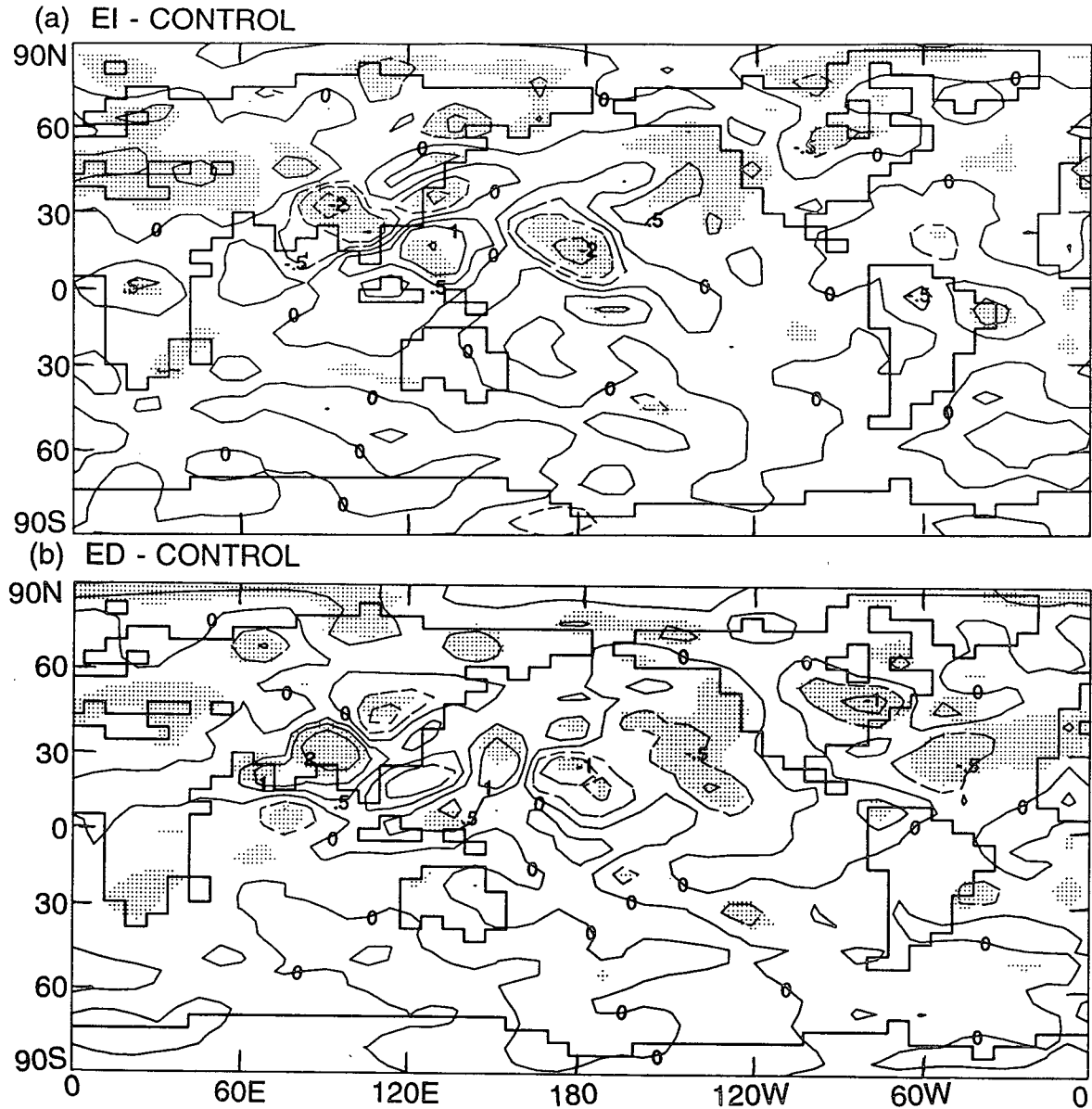


FIG. 12. As in Fig. 5 except for (a) EI minus control and (b) ED minus control.

subtropical experiments. Shifts in the storm track that could explain changes in precipitation over such large areas are not evident in the upper-tropospheric zonal wind (not shown), whose maximum remains over the same latitude in these regions, at least to the resolution of the R15 model. Instead they have to do with local and continental recycling of moisture. Many of these midlatitude regions typically have energy-limited evaporation during the winter, moisture-limited evaporation during the summer, and a transition period during the spring when the evaporation rate increases with increasing availability of energy. Some of this additional evaporated water is recycled into precipitation; the rest

contributes to moisture flux divergence out of the region, depleting the soil moisture (some of which was formerly stored as snow) and hastening the establishment of a moisture-limited state, in which local and continental recycling of moisture are no longer major contributors to precipitation. This entire process occurs earlier in the season with decreased surface albedo, limiting the precipitable water available from local evaporation during the summer, and later in the season with increased surface albedo, allowing more local recycling of moisture during the summer.

The exception to this lack of vertical motion and moisture convergence due to surface albedo perturba-

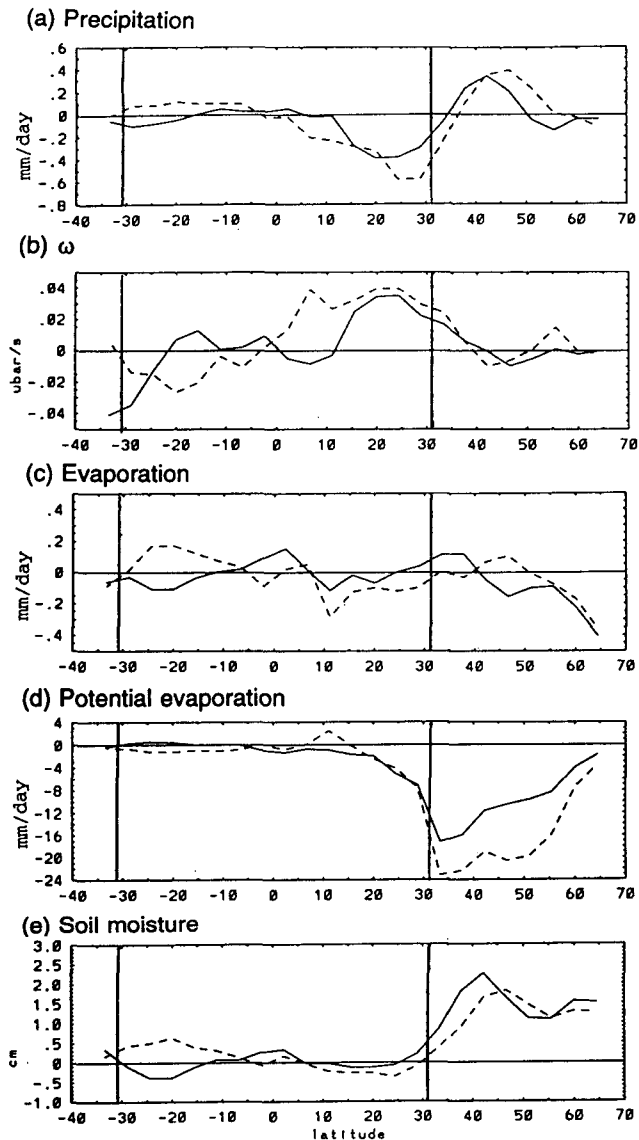


FIG. 13. As in Fig. 7 except the solid curves indicate EI minus control, and the dashed curves indicate control minus ED.

tions in the extratropics is in southern Asia, as indicated in Fig. 13. On the southern edge of the extratropical domain in Asia and extending outside of the domain, EI has decreased precipitation in the zonal mean (Fig. 13a), and ED has increased precipitation. That is, this part of Asia is acting more similarly to moist low-latitude regions because of the influence of the monsoon in this region. Again, it appears that a shift in the storm track cannot be used to explain these changes in precipitation. There are also various changes in precipitation in the Tropics and subtropics, with no distinguishable pattern.

Despite the increase in precipitation during JJA at midlatitudes in EI, evaporation is changed little (Fig.

13c). This is because decreased absorption of solar radiation cools the surface and reduces potential evaporation (Fig. 13d). Increased precipitation in experiment EI with little change in evaporation increases soil moisture (Fig. 13e), with geographical distribution similar to that shown for midlatitudes in Fig. 6. The soil moisture at these latitudes is decreased in ED by a similar amount.

#### d. Remote responses

Precipitation changes over the ocean also occur in response to surface albedo perturbations on land, particularly in the cases with global or subtropical perturbations (Figs. 5 and 8). In the decreased surface albedo cases, when increased diabatic heating causes enhanced atmospheric ascent over land in the Tropics and subtropics, it must be offset by descent elsewhere, primarily over the low-latitude oceans. Over the Atlantic, Pacific, and northern Indian Oceans, there is generally increased precipitation (with smaller-scale variations superimposed) in experiments GI and SI, and decreases in GD and SD. Changes in water vapor flux divergence result and feed back positively as discussed in subsection 5a1.

#### e. Linearity of results

By performing the set of eight experiments described here, it is possible to examine the linearity of the responses in two different senses. The first is linearity with respect to perturbations over partial domains, that is, whether or not the responses to surface albedo perturbations over the individual latitude belts add up to the response due to perturbation over the full global domain. This type of linearity establishes that at least at the scales used here for perturbation of surface albedo, perturbation of one domain will have approximately the same results regardless of the effects of perturbations at other locations. The second is linearity with respect to the amplitude and sign of the perturbation, which is addressed by comparison of responses to opposite perturbations in surface albedo. This type of linearity implies that the response can be directly scaled by the perturbation forcing it and gives us additional confidence in the model results.

The first type of linearity is addressed in Fig. 14, which shows the JJA zonal means over land only of several model variables for EI minus control, compared to the sum of EI minus control, SI minus control, and TI minus control. These graphs indicate linearity in that the sum of the responses to the latitude belt experiments equals, to a close approximation, the response in the global experiment. Remote responses in the latitude belt experiments, such as the spillover of precipitation responses into adjacent unperturbed regions, appear to be superimposed on local effects in the global perturbation experiments.

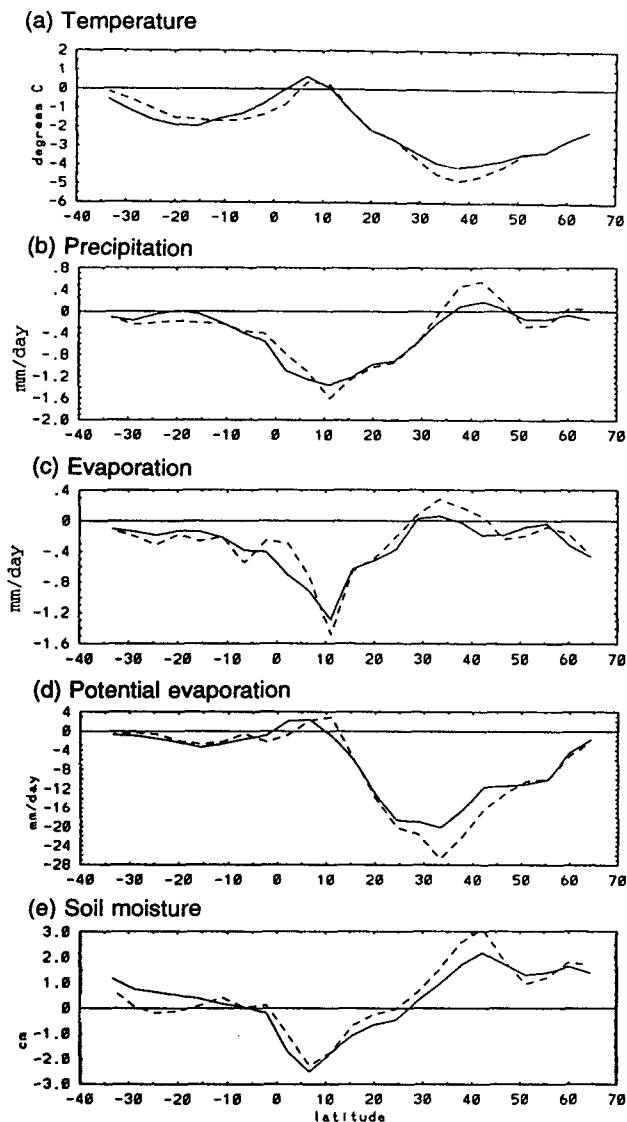


FIG. 14. Zonal means for June, July, and August over land only for GI minus control (solid curve) and for the sum of EI minus control, SI minus control, and TI minus control (dashed curve) of (a) surface air temperature, (b) precipitation, (c) evaporation, (d) potential evaporation, and (e) soil moisture.

Linearity with respect to the amplitude and sign of surface albedo perturbation has been addressed by superimposing zonal means of the pairs of experiments (Figs. 7, 11, and 13) and by the comparison of maps of geographical distribution of response to opposite perturbations. In general, these responses are nearly linear, but a number of exceptions exist, and several have been mentioned earlier in this text. The most notable is that in the Sahara, SD causes increases in precipitation and soil moisture during the summer that are much larger than the decreases caused by SI. In the annual mean, SI and SD both have increased soil moisture in

the Sahara. Both of these effects are simply because larger increases in precipitation and soil moisture can be achieved more easily, while decreases are strongly constrained by the very small ambient values.

## 6. Mixed layer experiment

Figure 15a shows the difference in surface air temperature during JJA between the mixed layer ocean cases, GIMO (in which surface albedo is increased by 0.05) and ConMO, and Fig. 15b shows the same quantity for GI5 minus the control case with prescribed sea surface temperature. The inclusion of a mixed layer ocean allows the air over the oceans to cool more, causing cooler air to advect from the oceans back over the land. Comparison of Figs. 15a and 15b indicates that the general effect of including a mixed layer ocean is to produce an additional decrease in surface temperature of  $1^{\circ}$ – $2^{\circ}$ C over both land and ocean. However, the change in land–ocean temperature gradient due to surface albedo perturbations is little affected. The only large departures are near Antarctica, where sea ice feedback is important. Nevertheless, thermally forced motion is qualitatively similar between the cases with prescribed sea surface temperature and mixed layer sea surface temperature. This also implies that changes in precipitation are qualitatively similar, which has been confirmed by model results that are not shown here.

The larger decrease in temperature when there is a mixed layer ocean is accompanied by some quantitative difference in the soil moisture response, although the qualitative features are maintained. Figure 16 shows that because the decreases in surface temperature and resulting decreases in potential evaporation are larger, the increases in soil moisture at midlatitudes during JJA are slightly larger under the mixed layer ocean formulation than with prescribed sea surface temperature, with some regions having increases greater than 3 cm. Again because potential evaporation is decreased by a larger amount, the decreases in soil moisture in the rainbelt of Africa, the south Asian monsoon region, and the Amazon Basin are smaller.

Figure 17 compares the pattern of change in JJA air temperature at the lowest model level due to the 0.05 reduction in land surface albedo with that due to doubling atmospheric carbon dioxide, both using a mixed layer ocean formulation. The comparison between the spatial distributions of these changes in temperature is motivated by the assertion of Charlson et al. (1992) that  $\text{CO}_2$  warming may be offset by the cooling effect of sulfate aerosol, which is crudely represented here by a change in surface albedo. Figure 17a shows the temperature change due to increased land surface albedo, normalized by the global mean decrease. Figure 17b shows the temperature change due to doubled  $\text{CO}_2$ , normalized by its global mean increase (results obtained from R. Wetherald, personal communication, 1992).

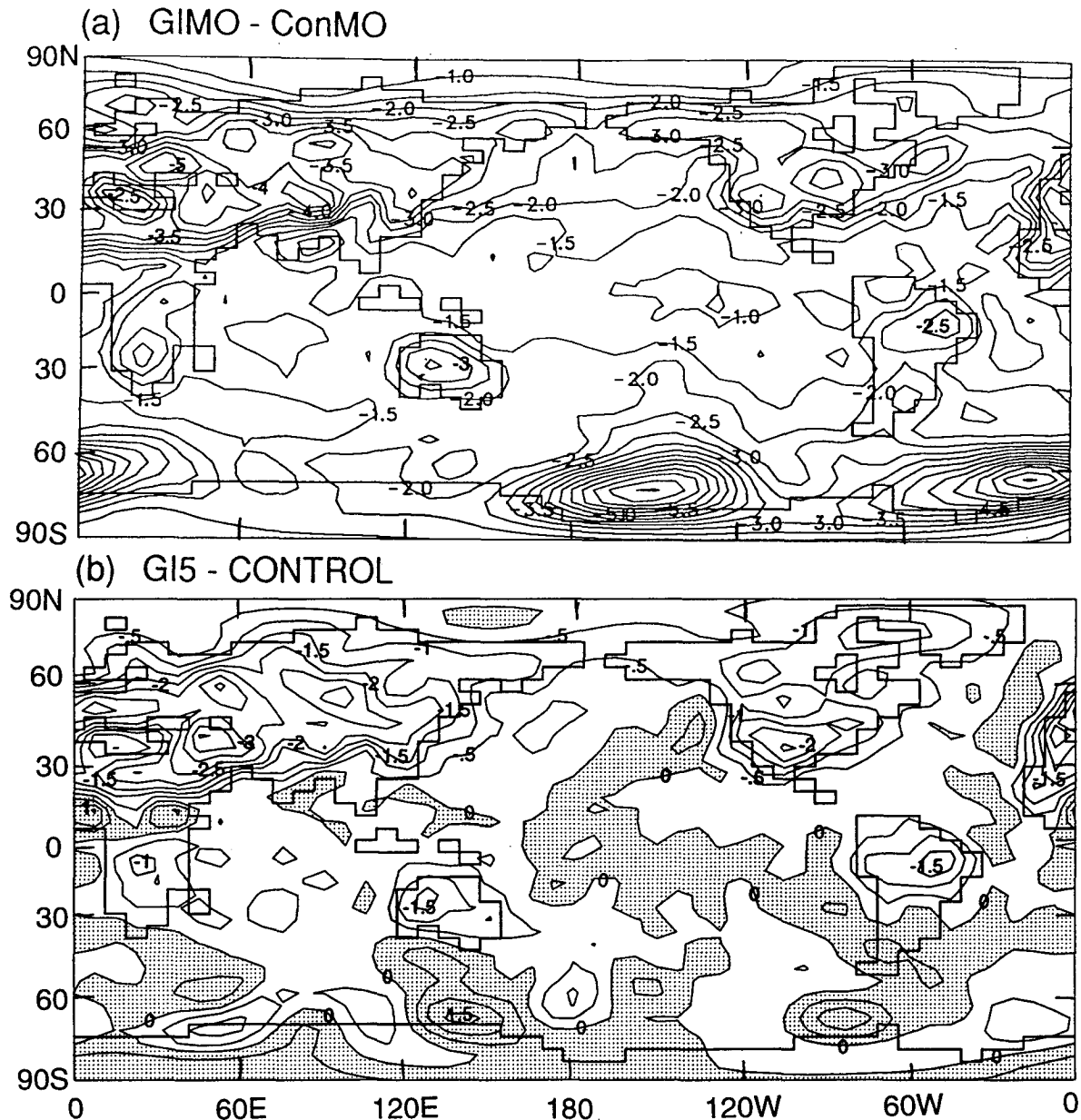


FIG. 15. JJA surface air temperature for (a) GIMO minus ConMO and (b) GI5 minus the control case with prescribed sea surface temperature. The contour interval is  $0.5^{\circ}\text{C}$ . Positive values are shaded. Smoothing is as in Fig. 3.

The two temperature change patterns share many features in common. Both have their largest changes in places affected by sea ice feedback during the Southern Hemisphere winter—in the Ross Sea and just east of the Weddell Sea. However, because of the artificial constraints imposed on sea ice thickness (see section 2), sea ice feedback must be viewed with caution. Both also have stronger temperature responses over land than over oceans, particularly in dry parts of the Northern Hemisphere midlatitudes such as southwestern North America and the Central Asian Desert. By

these indications, it can be said that if sulfate aerosols are distributed fairly uniformly over all land, the effects of aerosols will result in a similar spatial pattern of temperature changes to those due to greenhouse warming but of opposite sign.

However, the tendency for temperature change to occur primarily over land is much stronger in the increased surface albedo case (GIMO) than in the increased  $\text{CO}_2$  case. GIMO has temperature changes centered not only over the Northern Hemisphere continents, which are maximally affected by surface albedo

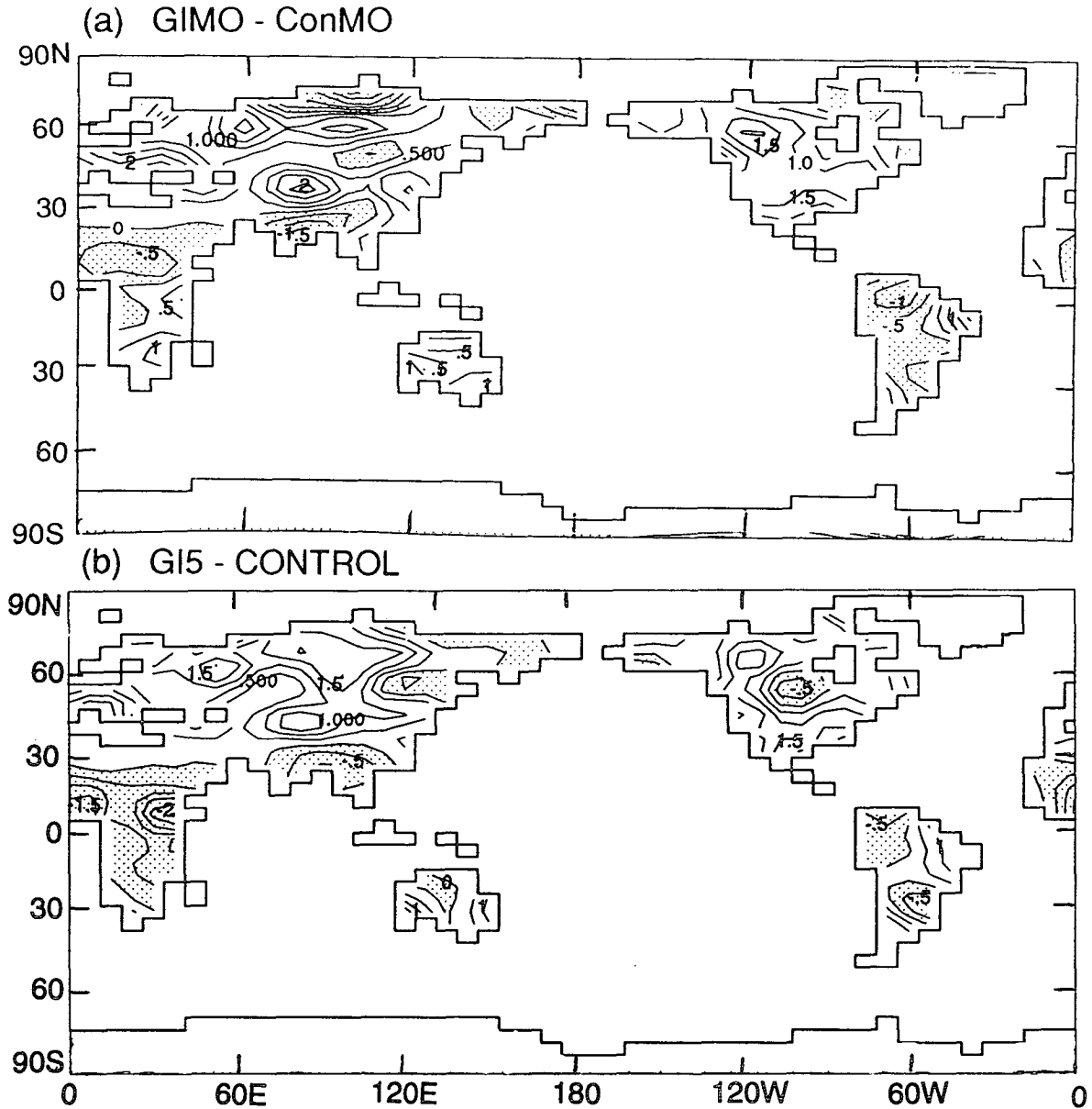


FIG. 16. JJA soil moisture for (a) GIMO minus ConMO and (b) G15 minus the control case with prescribed sea surface temperature. Contour interval is 0.5 cm. Smoothing is as in Fig. 3.

during the summer, but also Southern Hemisphere continents. On the other hand, the temperature increase due to doubled  $\text{CO}_2$  is much more concentrated in the polar regions of the winter hemisphere, with only small changes over the Southern Hemisphere continents.

In addition to not accurately representing the geographical distribution of atmospheric aerosols, this analog using a globally uniform perturbation in land surface albedo does not recognize that aerosols are more effective at reflecting solar radiation at large zenith angles (i.e., in the winter hemisphere and at high latitudes). Therefore, actual temperature responses to

aerosols in the high latitudes of the summer hemisphere and midlatitudes of the winter hemisphere may be larger than shown here, making the spatial pattern of aerosol cooling more like that of  $\text{CO}_2$  warming, except near the winter pole, where there is no sunlight and hence no response to aerosols.

## 7. Discussion and conclusions

It has been shown that prescribed perturbations in land surface albedo can result in different perturbations

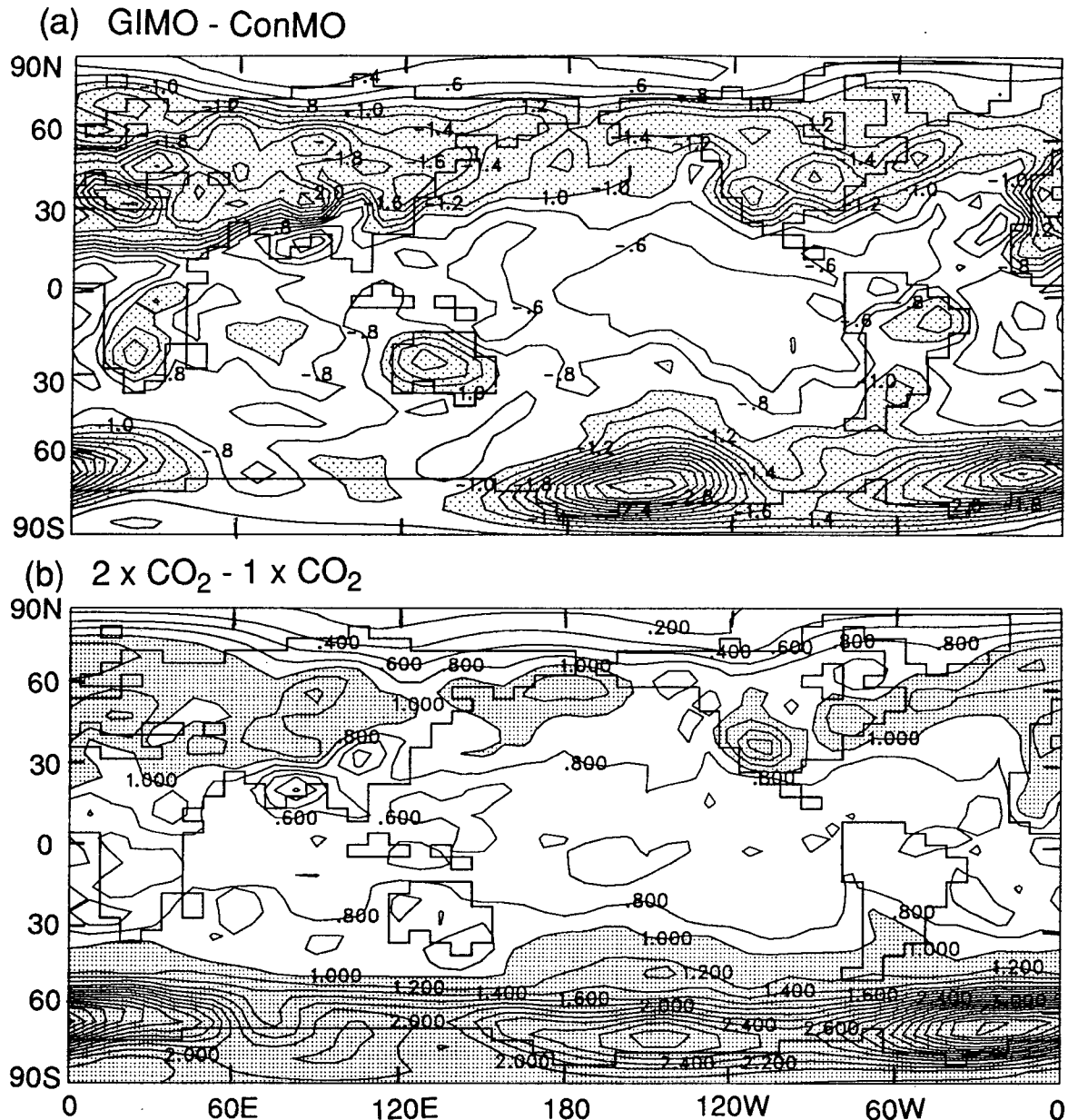


FIG. 17. JJA temperature in the lowest model level for (a) GIMO minus ConMO, normalized by the global mean decrease ( $2.1^{\circ}\text{C}$ ), and (b) a doubled  $\text{CO}_2$  case minus control case, normalized by the global mean increase ( $3.8^{\circ}\text{C}$ ). Changes of magnitude greater than the global mean are indicated by shading. Smoothing is as in Fig. 3.

in soil moisture depending on latitude, ambient soil moisture, and other conditions.

The precipitation response to surface albedo perturbations in these simulations is large in the tropical rainbelt and, during the rainy season, in the seasonally moist parts of the subtropics. This results from two cooperating factors. The first is that when surface albedo is decreased, the additional energy available at the surface leads to increased evaporation. This moisture is mostly added to convective systems in the vicinity of

its origin, thus increasing precipitation. In addition to this, the latent heat released by this precipitation, along with any additional sensible heat added to the atmosphere, leads to upward motion of the atmosphere, which provides a balancing adiabatic cooling. Associated with this upward motion is convergence of moist air at low levels and dry air divergence in the upper troposphere, yielding net water vapor flux convergence, another mechanism that enhances precipitation. This water vapor flux convergence is key to producing

large precipitation responses to albedo perturbations. The opposite occurs with increased surface albedo; decreased evaporation and relative divergence of water vapor flux due to downward motion reduce precipitation. It should also be noted that the use of the moist convective adjustment scheme in this model may have a large effect on the amplitude of this water vapor flux convergence.

It must be noted that the change in net radiative heating of the surface is not solely due to the surface albedo's direct effect on solar absorption. Accompanying changes in cloudiness strongly moderate the effect on surface solar absorption, but this is partially offset by the clouds' effect on downward longwave radiation. However, the net effect of the change in cloudiness, in comparison with a case with constant cloudiness, has not been evaluated.

In arid subtropical regions, very low ambient soil moisture means that perturbed surface albedo results in only a small change in evaporation. The dryness of near-surface air also limits the change in water vapor convergence. Therefore, precipitation changes resulting from changes in surface albedo over subtropical deserts are smaller than over the tropical rainbelts.

In the midlatitudes, there tends not to be strong vertical motions to compensate for diabatic heating. Thus the responses in precipitation due to surface albedo perturbations are small.

At all latitudes, there is the additional effect by which decreased surface albedo increases the potential evaporation, which tends to dry out the soil. In the midlatitudes, where there is little accompanying change or a slight reduction in precipitation, the net effect on soil moisture is drying. In the tropical rainbelts, the large increase in precipitation overcomes this effect. Arid subtropical regions have smaller changes in precipitation, so the net change in soil moisture is smaller there than in the rainbelts.

Perturbations in surface albedo and resulting changes in low-latitude rainfall are associated with alterations of the large-scale zonal overturning between land and ocean. This causes precipitation over the oceans, particularly at low latitudes, to be perturbed in the sense opposite to the changes over land. That is, when surface albedo on land is decreased, precipitation over the ocean is decreased, and vice versa.

Thermal forcing of atmospheric circulation may be different if sea surface temperatures are allowed to respond to changes in heat advection from the continents. Therefore, additional experiments were performed using a mixed layer ocean formulation. When using this formulation, the land-ocean temperature gradient is little affected, since decreases in temperature occur over both land and ocean due to increased land surface albedo. This leaves the circulation and precipitation responses qualitatively similar to those with prescribed sea surface temperature. The increase in soil moisture with increased surface albedo at midlatitudes is ampli-

fied, and the decrease at lower latitudes is slightly diminished. The qualitative agreement between results from surface albedo perturbations with and without mixed layer ocean formulation indicate that the more detailed results shown here from experiments with prescribed sea surface temperature are a good indicator of the effects on an atmosphere that is interactive with the ocean, when it is assumed that there is no accompanying change in oceanic heat transport.

Increased surface albedo with a mixed layer ocean is used as a simple analog for elevated amounts of lower-tropospheric aerosols (see Charlson et al. 1992; Penner et al. 1992). The spatial distribution of changes in surface air temperature due to increased surface albedo with a mixed layer ocean are similar to those due to increased atmospheric CO<sub>2</sub> in having its largest changes where sea ice feedback occurs in the winter hemisphere and in having larger changes over land than over most oceans.

The results shown here are consistent with those of Charney (1975), Charney et al. (1977), Sud and Fennesy (1982), and Sud and Molod (1988). New results include the net effect on soil moisture, considered over a time period sufficient to eliminate dependence on initial conditions and to increase signal to noise ratio, and the qualitative similarity between results with prescribed sea surface temperatures and the mixed layer ocean formulation. The results of tropical deforestation simulations by Lean and Warrilow (1989), Nobre et al. (1991), and Dickinson and Henderson-Sellers (1988) appear to be consistent with this study in terms of precipitation changes, although direct comparison is made difficult by the comparative complexity of their land surface parameterizations and the number of parameters that were changed in simulating deforestation. Additional work, applying the results of these deforestation studies to a simple dynamical model of the tropical atmosphere was undertaken by Eltahir and Bras (1993), who found, as in this paper, that forcing due to the release of latent heat in the atmosphere is very important in determining the overall response to land surface perturbations.

The qualitative aspects of the major physical mechanisms discussed here are believed to be independent of the parameterization schemes used in the model, although different schemes will involve different feedbacks. Therefore, it is likely that models with more detailed parameterizations of land-surface processes will have qualitatively similar sensitivity to perturbations in surface albedo alone, although details of the response may differ.

When it is assumed that high soil moisture leads to plentiful vegetation and low surface albedo, the results here suggest that heavy precipitation in tropical rainbelts reinforces itself by lowering surface albedo, that is, positive feedback. Weaker positive feedback may occur in subtropical regions, and negative feedback may occur at midlatitudes. These feedbacks will be ex-

plored in Lofgren (1995) using a simple model of surface albedo's response to simulated climate.

*Acknowledgments.* This paper resulted from work done for my Ph.D. thesis at Princeton University. It would not have been possible without the guidance of Dr. Syukuro Manabe. This work was supported through a National Science Foundation Graduate Student Fellowship and a NASA Global Change Graduate Student Fellowship. The Geophysical Fluid Dynamics Laboratory and the Great Lakes Environmental Research Laboratory provided the necessary computing resources. N.-C. Lau, C. Milly, V. Ramaswamy, T. Croley, and P. Dirmeyer are gratefully acknowledged for helpful discussions and comments on early versions of the manuscript, and two anonymous reviewer gave additional helpful remarks. A. Broccoli, R. Wetherald, T. Delworth, and R. Stouffer gave assistance in running the GCM. P. Tunison, J. Varanyak, and C. Rafael assisted in preparation of several figures.

#### REFERENCES

- Carson, D. J., and A. B. Sangster, 1981: The influence of land-surface albedo and soil moisture content on general circulation model simulations. GARP/WCRP Report 2, 5.14–5.21.
- Charlson, R. J., S. E. Schwartz, J. M. Hales, R. D. Cess, J. A. Coakley Jr., J. E. Hansen, and D. J. Hofmann, 1992: Climate forcing by anthropogenic aerosols. *Science*, **255**, 423–430.
- Charney, J. G., 1975: Dynamics of deserts and drought in the Sahel. *Quart. J. Roy. Meteor. Soc.*, **101**, 193–202.
- , W. J. Quirk, S.-H. Chow, and J. Kornfield, 1977: A comparative study of the effects of albedo changes on drought in semi-arid regions. *J. Atmos. Sci.*, **34**, 1366–1385.
- Chervin, R. M., 1979: Response of the NCAR general circulation model to changed land surface albedo. *Report of the JOC Study Conference on Climate Models: Performance, Intercomparison, and Sensitivity Studies*. GARP Publications Series, No. 22, Vol. I, 563–581.
- CLIMAP Project Members, 1981: Seasonal reconstructions of the earth's surface at the last glacial maximum. Geological Society of America Map and Chart Series, MC-36.
- Cunnington, W. M., and P. R. Rowntree, 1986: Simulations of the Saharan atmosphere—Dependence on moisture and albedo. *Quart. J. Roy. Meteor. Soc.*, **112**, 971–999.
- Dickinson, R. E., and A. Henderson-Sellers, 1988: Modelling tropical deforestation: A study of GCM land-surface parameterizations. *Quart. J. Roy. Meteor. Soc.*, **114**, 439–462.
- Eltahir, E. A. B., and R. L. Bras, 1993: On the response of the tropical atmosphere to large-scale deforestation. *Quart. J. Roy. Meteor. Soc.*, **119**, 779–793.
- Frank, W. M., and J. Molinari, 1993: Convective adjustment. *The Representation of Cumulus Convection in Numerical Models*, Meteor. Monogr., No. 24, K. A. Emanuel and D. J. Raymond, Eds., Amer. Meteor. Soc., 101–105.
- Gordon, C. T., and W. F. Stern, 1982: A description of the GFDL global spectral model. *Mon. Wea. Rev.*, **110**, 625–644.
- Held, I. M., 1985: Stationary and quasi-stationary eddies in the extratropical troposphere: Theory. *Large-Scale Dynamical Processes in the Atmosphere*, B. J. Hoskins and R. P. Pearce, Eds., Academic Press, 127–168.
- Jaeger, L., 1976: Monthly precipitation maps for the entire earth (in German). *Ber. Deutsch Wetterdienstes*, **18**(139), 38 pp.
- Kukla, G., and D. Robinson, 1980: Annual cycle of surface albedo. *Mon. Wea. Rev.*, **108**, 56–68.
- Lacis, A. A., and J. E. Hansen, 1974: A parameterization for the absorption of solar radiation in the earth's atmosphere. *J. Atmos. Sci.*, **31**, 118–133.
- Lean, J., and D. A. Warrilow, 1989: Simulation of the regional climatic impact of Amazon deforestation. *Nature*, **342**, 411–413.
- Lofgren, B. M., 1995: Surface albedo–climate feedback simulated using two-way coupling. *J. Climate*, **8**, 2543–2562.
- Manabe, S., 1969: Climate and ocean circulation. Part I: The atmospheric circulation and the hydrology of the earth's surface. *Mon. Wea. Rev.*, **97**, 739–774.
- , J. Smagorinsky, and R. F. Strickler, 1965: Simulated climatology of a general circulation model with a hydrologic cycle. *Mon. Wea. Rev.*, **93**, 769–798.
- Milly, P. C. D., 1992: Potential evaporation and soil moisture in general circulation models. *J. Climate*, **5**, 209–226.
- Nobre, C. A., P. J. Sellers, and J. Shukla, 1991: Amazonian deforestation and regional climate change. *J. Climate*, **4**, 957–988.
- Penner, J. E., R. E. Dickinson, and C. A. O'Neill, 1992: Effects of aerosol from biomass burning on the global radiation budget. *Science*, **256**, 1432–1434.
- Rodgers, C. D., and C. D. Walshaw, 1966: The computation of infrared cooling rate in planetary atmospheres. *Quart. J. Roy. Meteor. Soc.*, **92**, 67–92.
- Stone, H. M., and S. Manabe, 1968: Comparison among various numerical models designed for computing infrared cooling. *Mon. Wea. Rev.*, **96**, 735–741.
- Sud, Y. C., and M. Fennessy, 1982: A study of the influence of surface albedo on July circulation in semi-arid regions using the GLAS GCM. *J. Climatol.*, **2**, 105–125.
- , and A. Molod, 1988: A GCM simulation study of the influence of Saharan evapotranspiration and surface-albedo anomalies on July circulation and rainfall. *Mon. Wea. Rev.*, **116**, 2388–2400.
- Wetherald, R. T., and S. Manabe, 1980: Cloud cover and climate sensitivity. *J. Atmos. Sci.*, **37**, 1485–1510.